Chemical Geology 509 (2019) 234–248

Contents lists available at ScienceDirect

Chemical Geology

journal homepage: www.elsevier.com/locate/chemgeo

Approach to trace hidden paleo-weathering of basaltic crust through decoupled Mg–Sr and Nd isotopes recorded in volcanic rocks

Heng-Ci Tian[a,b,*], Wei Yang[a,b], Shu-Guang Li[c,**], Hai-Quan Wei[d], Zhuo-Sen Yao[e], Shan Ke[c]

[a] Key Laboratory of Earth and Planetary Physics, Institute of Geology and Geophysics, Chinese Academy of Sciences, Beijing 100029, China
[b] Institutions of Earth Science, Chinese Academy of Sciences, Beijing 100029, China
[c] State Key Laboratory of Geological Processes and Mineral Resources, China University of Geosciences, Beijing 100083, China
[d] Institute of Geology, China Earthquake Administration, Beijing 100029, China
[e] Key Laboratory of Mineral Resources, Institute of Geology and Geophysics, Chinese Academy of Sciences, Beijing 100029, China

ARTICLE INFO

Editor: Anthony Dosseto

Keywords:
Hidden paleo-weathering of crust
Sr-Nd-Mg isotopes
AFC processes
Chemical weathering
Changbaishan volcanic rocks

ABSTRACT

On Earth, chemical weathering of basaltic rocks not only modulates the climate change, but also plays a crucial role on the ocean oxygenation and ecosystem evolution. Records of paleo-weathered crusts are a challenge to identify because they are obscured by subsequent alteration processes and buried by the newly formed volcanic lavas. However, late formed volcanic rocks theoretically could record previously weathered crust via their assimilation and fractional crystallization (AFC) processes. Here, we present a systematic study on major, trace elements and Sr-Nd-Mg isotopes in a suite of Changbaishan early formed basalts and late erupted trachytes from Northeast China. Detailed evidence of field observation, geochemical signature and rhyolite-MELTS simulations suggest that trachytes mainly originated from deep fractional crystallization of basaltic melts. The low abundant trachytes from the stratigraphic layer above the basalts display decoupled Mg–Sr and Nd isotopes. δ^{26}Mg and $^{87}Sr/^{86}Sr$ in trachytes range from −0.27 up to +0.94‰ (the heaviest isotopic composition ever reported for Mg in the igneous rocks) and 0.70490 to 0.71065, respectively, which are significantly elevated relative to that of their mantle source. However, they preserved mantle source-like $^{143}Nd/^{144}Nd$ (0.512584 to 0.512656) ratios. These unusual characteristics cannot be explained by thermal diffusion, fractional crystallization or simple crustal contamination processes. Specifically, δ^{26}Mg correlates positively with SiO_2 and $^{87}Sr/^{86}Sr$, and negatively with MgO, CaO, Al_2O_3, Sr and Nb/U indicators. The highly elevated Mg and Sr isotopes but limited Nd isotopic changes in trachytes require a component to be the relatively younger weathering residue of basaltic rocks. Taking this component as a wall rock endmember, the well-developed above correlations can be best modelled by AFC processes. This reflects that some trachytes in the aftermath of AFC processes almost fully lost their primary source characteristics, but inherited the intense chemical weathering signature of basalts. This event probably occurred in the middle Miocene as studies of paleosols showed humid and warm climate during that period after the initial eruption of Changbaishan basalts. Therefore, our study as a specific case for the first time provides an efficient way to explore paleo-weathering of basaltic crusts buried in the Earth's surface, through comprehensive investigating Mg, Sr and Nd isotopes of volcanic rocks developed in the late stage of a volcano cone.

1. Introduction

Chemical weathering of silicates, especially the large continental flood basalt provinces around the world, serves as a long-term sink of atmospheric CO_2 (Louvat and Allègre, 1997, 1998; Dessert et al., 2001, 2003). It regulates climate through the greenhouse effect of CO_2 over geological time, providing a negative climate feedback (e.g. Berner et al., 1983; Dessert et al., 2003; Ibarra et al., 2016; Li et al., 2016a). For example, previous studies have demonstrated that basaltic rocks with faster weathering rate than other silicates account for as much as 30 to 35% of modern CO_2 consumption by global silicate weathering, while they are estimated to occupy less than ~5% of the global land surface (e.g. Gaillardet et al., 1999; Dessert et al., 2003; Hartmann et al., 2009; Hartmann and Moosdorf, 2012; Moon et al., 2014; Balagizi et al.,

* Correspondence to: H.-C. Tian, Key Laboratory of Earth and Planetary Physics, Institute of Geology and Geophysics, Chinese Academy of Sciences, Beijing 100029, China.
** Corresponding author.
E-mail addresses: hctian@mail.iggcas.ac.cn (H.-C. Tian), lsg@ustc.edu.cn (S.-G. Li).

https://doi.org/10.1016/j.chemgeo.2019.01.019
Received 3 August 2018; Received in revised form 4 January 2019; Accepted 17 January 2019
Available online 03 February 2019
0009-2541/ © 2019 Elsevier B.V. All rights reserved.

2015). Additionally , their weathering rates are high in tropical and subtropical environment, and gradually decrease towards middle- and high-latitude (e.g. Kent and Muttoni, 2013; Balagizi et al., 2015; Dessert et al., 2015). This implies that basalt weathering plays a significant role for the long-term global carbon cycle. However, most studies on continental basalts weathering focus on the modern environment (Dessert et al., 2003; Li et al., 2016a). The paleo-weathered basaltic events received much less attention, which have been linked directly or indirectly to the paleoclimate change, ocean oxygenation, ecosystem changes or mass extinction (Dessert et al., 2003; Hartmann and Moosdorf, 2012; Sun et al., 2018; Yang et al., 2018). Knowledge of the past variability of climate in continental crust could be obtained through directly studying the paleo-weathered crust, which can help to inform our understanding of past climate change and provide the baseline for ongoing and future climate change. However, one of the main difficulties of studying basaltic rocks paleo-weathering is that weathered crusts were always covered by the newly formed volcanic lavas or sediments and were also modified by later geological processes. Many volcanoes worldwide not only have accumulated a lot of basaltic lavas in the deeper region, but also commonly accompanied with small amounts of intermediate-felsic rocks at the shallow part (e.g. Chung and Jahn, 1995; Bryan and Ernst, 2008; Dufek and Bachmann, 2010). Theoretically, the late formed intermediate-felsic rocks can record wallrocks information via crustal contamination processes during magma ascent and emplacement. More importantly, selecting sensitive proxies are the keys to ascertain the nature and intensity of past silicates weathering events.

Magnesium is a water-soluble major element that occurs in continental crust and mantle (e.g. McDonough and Sun, 1995; Rudnick and Gao, 2003). Mg can easily fractionate at low-temperature, while Mg will minimally fractionate in high-temperature magmas (e.g. Teng, 2017 and references therein). For example, during low-temperature continental weathering, the residual of sedimentary rocks (e.g. shales, pelites, and loess) and silicate rocks generally enrich heavy Mg isotopes relative to the un-weathered protolith, making the light Mg isotopes enter into the hydrosphere (Li et al., 2010; Opfergelt et al., 2012; Liu et al., 2014; Wimpenny et al., 2014). Furthermore, during the chemical weathering, Sr behaves much more active than Nd and is easily removed from the primary rocks (e.g. Nesbitt et al., 1980; McCulloch et al., 1981; Ma et al., 2007). During chemical weathering, significant changes of $^{87}Sr/^{86}Sr$ have been reported by most studies (e.g. McCulloch et al., 1981; Ma et al., 2010). This can be attributed to differential decomposition of minerals containing heterogeneous $^{87}Sr/^{86}Sr$ ratios (Blum and Erel, 1995; Negrel, 2006) or input of extraneous Sr with high $^{87}Sr/^{86}Sr$ ratios from aeolian deposits or groundwater (Price et al., 1991; Stewart et al., 2001; Kurtz et al., 2001; Dia et al., 2006; Ma et al., 2010). In contrast, due to the much high atomic numbers and weak immobility, Nd isotopes are unlikely to be fractionated by incongruent weathering unless some aeolian dusts involved into the weathering saprolite (Ma et al., 2010; Liu et al., 2013). Additionally, the best efficient approach to explore paleo-weathered crusts may be via investigating the late-erupted intermediate-felsic lavas laying on top of a volcano cone. That is because these volcanic lavas will inevitably assimilate the early erupted basalts during their ascent (Depaolo, 1981), and generally have low volume relative to early erupted volcanic lavas. Specifically, if the early basalts experienced intense weathering, it will be inherited by the late formed volcanic lavas.

The volcanic lavas exposed in Changbaishan and surrounding areas from Northeast (NE) China (Fig. 1a), are an excellent natural laboratory to resolve this issue. That is because (1) Changbaishan stratovolcano is composed of multi-stage eruptions from ~20 Ma until one thousand years ago (Zhang et al., 2018 and references therein) and (2) previous studies demonstrated that East Asia experienced several strong summer monsoon and tropical-like climate during the Miocene (e.g. Zou et al., 2004; Sun et al., 2015; Meng et al., 2018). In this paper, we investigate the Sr-Nd-Mg isotopes and trace elements of twelve early erupted alkali basalts and fourteen late-erupted trachytes (Fig. 1b), to understand how the paleo-weathered basaltic crust affects isotopic behaviors, to reveal the paleoclimate change in NE China and more importantly to obtain a general pathway to study the paleo-weathered crust.

2. Geological setting and samples

The Changbaishan volcanic area is located in NE China, between the Japan Sea back-arc basin and the Songliao Basin (Fig. 1a) and belongs to active Cenozoic volcanoes in China (e.g. Liu, 1999, 2000; Wei et al., 2003). Many faults have occurred in this area, such as Mishan-Dunhua Fault, Tianchi-Tumenjiang Fault and Tianchi-Baishan Fault (Zhang et al., 2002). Three large volcanic systems compose the Changbaishan volcanic area: Tianchi (China-North Korea), Wangtian'e (China) and Baotaishan (North Korea). The Changbaishan volcanic area is composed of an early basaltic shield (ca. ~2.8 to 0.31 Ma), middle trachyte composite cone (ca. 1.1 to 0.1 Ma) and the final eruption of the Holocene ignimbrite (< 0.1 Ma) rocks (or alkali rhyolites) based on the Ar−Ar, K−Ar and U−Th dating (e.g. Liu and Wang, 1982; Wei et al., 2003, 2007; Fan et al., 2006; Zou et al., 2010, 2014; Liu et al., 2015; Ramos et al., 2016), on top of Archean metamorphic rocks and Mesozoic granites. This basaltic shield is composed of almost entirely of lavas flows. Based on the statistics, the lava shield covers an area of ~ 20,000 km^2, extending to 50 and 100 km in different directions (Wei et al., 2003).

There are still controversies over the origin of the volcanic rocks. Cenozoic magmatic activity in NE China has been interpreted as the result of decompression melting of the asthenosphere (e.g. Zou et al., 2003, 2008; Zhao et al., 2009; Kuritani et al., 2011; Tang et al., 2014; Choi et al., 2017). This explanation is supported by the high-resolution seismic tomography of a plume-like shape beneath the Changbaishan area (Zhao et al., 2009; Tang et al., 2014). Many models plausibly explain the slightly enriched Sr-Nd-Pb isotopes in Changbaishan basalts, including metasomatism from ancient stagnant slab (Kuritani et al., 2011), subduction of the Pacific slab in the mantle transition zone (410–660 km; Zhao et al., 2009), assimilated crustal materials (Zou et al., 2008) or the enriched lithospheric mantle (Chen et al., 2007). In contrast, most previous studies have suggested that trachytes formed from the prolonged fractional crystallization of minerals (olivine ± pyroxene ± plagioclase) from the alkali basalts, together with assimilation of some crustal materials (e.g. Xie et al., 1988; Liu et al., 1998, 2015; Li et al., 2004; Guo et al., 2015, 2016; Park et al., 2016).

In this study, twelve alkali basalts (ca. 1.91 to 0.18 Ma) and fourteen trachytes (ca. 1.14 to 0.12 Ma) (Table 1) were collected from Changbaishan volcanic area (Fig. 1b). Their lithology and major elements are reported by previous studies (Wei et al., 2007; Sun et al., 2008; Chen, 2013). Except for one sample with slightly high LOI (2.57 wt%), all the other basalts and trachytes display low LOI ranging from −0.39 to 0.95 wt% (Table 1), reflecting they are not affected by alteration. These alkali basalts are mainly porphyritic or holocrystalline, containing olivine (< 5%), augite (3–5%) and plagioclase (< 15%) phenocrysts (Chen, 2013). They have low MgO (3.60–5.53 wt%), high SiO_2 (48.67–52.14 wt%), Na_2O (3.64–4.05 wt%) and K_2O (1.88–2.34 wt%) contents. In contrast, the trachytes have characteristically trachytic texture, with the phenocrysts of plagioclase (10–30%) and minor pyroxene (< 3%). They are characterized by low MgO (0.05–1.02 wt%) and CaO (0.55–2.40 wt%), variable Al_2O_3 (12.25–17.91 wt%) and total FeO (4.81–7.21 wt%) (Chen, 2013).

3. Analytical methods

3.1. Trace elemental analyses

The chemical procedure was conducted in an ultra-clean laboratory at the State Key Laboratory of Geological Process and Mineral

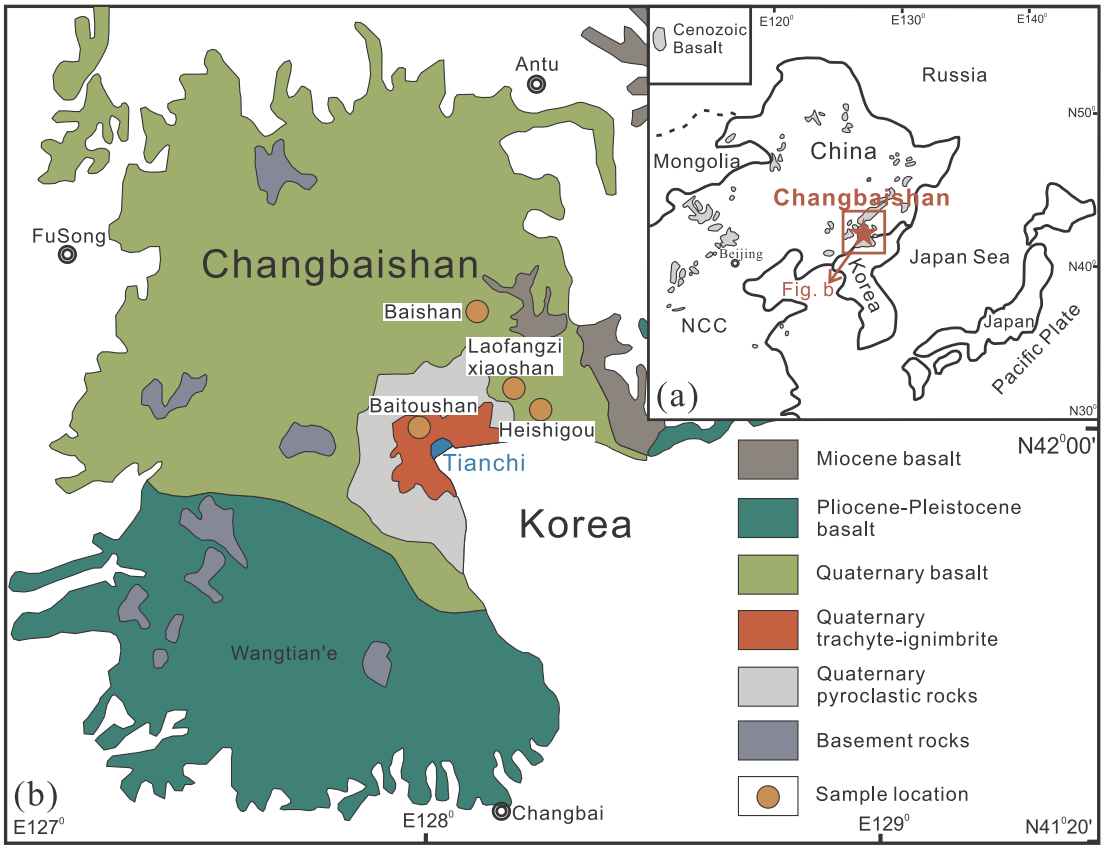

Fig. 1. (a) Map showing the location of Changbaishan and the distribution of Cenozoic volcanic rocks in Northeast China (modified from Wei et al., 2003). (b) The distribution of Cenozoic basalts and trachyte-ignimbrite in Changbaishan area (modified from Fan et al., 2006 and Guo et al., 2014). Four orange circles represent the locations of basalts and trachytes collected in this study.

Resources, China University of Geosciences (Beijing) (CUGB). Trace element concentrations were determined with inductively coupled plasma mass spectrometry (ICP-MS) using an *ELEMENT* instrument at the Institute of Geology and Geophysics, Chinese Academy of Sciences (IGGCAS). Two reference materials GSR1 and GSR3 were also analyzed to monitor the entire chemical procedure and instrument stability. The measured values of GSR1 and GSR3 are consistent with the recommended values (Table 2). Precision and accuracy is better than 5% for most of the trace elements.

3.2. Sr-Nd-Mg isotopic analyses

Whole-rock Sr—Nd isotopic compositions were analyzed at IGGCAS using a *Triton Plus* thermal ionization mass spectrometer (TIMS) instrument, following the previously established methods (Li et al., 2015, 2016b). Sr and Nd were separated using the classical two-step ion exchange chromatographic method. Due to the high Rb/Sr (> 6) in some samples (008–7, I-15-1, I-25-1, 2–15-2, 2(1)S, I-7-2, I-8-1, I-8-2 and I-101-1), the same chemical separation column was achieved twice. Isotopic ratios corrected for mass fractionation were normalized to $^{86}Sr/^{88}Sr = 0.1194$ and $^{146}Nd/^{144}Nd = 0.7219$, respectively. The standard materials NBS-987 and JNdi-1, were also used to evaluate the instrument stability during data collection. The results were $^{87}Sr/^{86}Sr = 0.710256 \pm 0.000020$ (2SD, $n = 2$) for NBS-987 and $^{143}Nd/^{144}Nd = 0.512112 \pm 0.000007$ (2SD, n = 2) for JNdi-1. Basalt standard (BCR-2) was also analyzed and yielded $^{87}Sr/^{86}Sr = 0.705000 \pm 0.000014$ (2σ) and $^{143}Nd/^{144}Nd = 0.512652 \pm 0.000008$ (2σ). These results are in good agreement with recommended values on GeoREM (http://georem.mpch-mainz.gwdg.de/).

Magnesium isotope analyses were carried out using a *Neptune* multi collector inductively coupled plasma mass spectrometer (MC-ICP-MS) at CUGB, based on the method described in previous studies (e.g. Teng et al., 2010; Ke et al., 2016). For chemical procedure, powdered samples in Savillex beakers were totally dissolved in concentrated HF-HNO_3-HCl. All dried sample residues were dissolved in 1 N HNO_3 for Mg separation. Samples containing ~10 μg Mg were separated by cation exchange chromatography using Bio-Rad 200–400 mesh AG50W-X8 pre-clean resin and eluted using 1 N HNO_3 at a rate of 1 mL/30 min. Considering higher Na_2O and Al_2O_3 content than MgO content in some of the trachytes (samples I-15-1, 2(1)S, I-7-2, I-8-2 and I-101-1), the same chemical separation column was achieved three times. This was also applied to the two standards of AGV-2 and GSP-2. After three passes, the abundances of Ti, Al, Fe, Ca, Na and K relative to Mg in each sample solution was measured and the cation/Mg (mass/mass) ratios were < 0.05. The Mg yield after three passes was > 99.0%.

Purified Mg solutions were analyzed with the sample-standard bracketing method to correct for instrumental mass bias. The long-term reproducibility based on analyses of natural materials and synthetic pure Mg solution is better than 0.06‰ for $\delta^{26}Mg$ and 0.05‰ for $\delta^{25}Mg$ (Ke et al., 2016). The Mg isotopes are expressed as $\delta^{25}Mg$ and $\delta^{26}Mg$, where $\delta^{25,26}Mg_{sample} = [(^{25,26}Mg/^{24}Mg)_{sample}/(^{25,26}Mg/^{24}Mg)_{DSM3}-1] \times 1000$ (‰), where DSM3 is a solution of pure Mg metal (Galy et al., 2003). The data is presented in Table 3. The $\Delta^{25}Mg'$ ($\Delta^{25}Mg' = \delta^{25}Mg' - 0.521 \times \delta^{26}Mg'$, where $\delta^{25,26}Mg' = 1000 \times \ln[(\delta^{25,26}Mg + 1000)/1000]$; Young and Galy, 2004) values are within 0 ± 0.05‰ (Table 3). Thus, only the $\delta^{26}Mg$ values will be used in the discussion. Four USGS rock standards analyzed during the course of this study yielded $\delta^{26}Mg$ values of −0.27 ± 0.06‰ for BHVO-2, −0.20 ± 0.09‰ for BCR-2, −0.15 ± 0.04‰ for AGV-2 (2SD, $n = 2$) and + 0.05 ± 0.06‰ for GSP-2 (2SD, n = 2), which are consistent with those reported in previous studies (e.g. Teng et al., 2007, 2015; Opfergelt et al., 2012; An et al., 2014; Ke et al., 2016).

Table 1
Major element data and age for the Changbaishan basalts and trachytes, Northeast China.

Sample[a]	SiO_2	TiO_2	Al_2O_3	Fe_2O_3[b]	MnO	MgO	CaO	Na_2O	K_2O	P_2O_5	LOI	Total	CIA[c]	Mg#[b]	Age(Ma)[d]
Basalts															
T2-1	48.67	3.33	16.45	13.98	0.15	3.60	6.75	3.73	2.31	0.65	0.76	100.38	44.0	37.6	
I-75-1	49.38	3.76	15.86	11.32	0.14	4.51	7.87	3.65	2.29	0.71	-0.28	99.21	41.0	48.2	1.1
I-98-1	50.86	3.53	15.77	11.69	0.14	4.12	7.61	3.95	2.30	0.72	0.50	101.19	40.8	45.1	1.9
I-99-1	50.92	3.53	15.92	11.39	0.14	3.97	7.54	3.79	2.34	0.69	-0.39	99.84	41.4	44.9	0.2
T2-5	49.46	3.32	15.91	12.00	0.15	4.96	7.62	3.79	2.15	0.74	0.39	100.49	41.5	49.1	0.6
I-55-1	49.59	3.29	16.20	11.56	0.15	4.67	7.65	3.64	2.18	0.69	-0.21	99.41	42.1	48.5	1.0
I-34-1	50.30	2.85	16.06	11.44	0.15	5.47	7.54	3.79	1.92	0.59	0.43	100.54	42.1	52.8	0.5
I-47-1	50.72	2.70	15.90	11.26	0.14	5.53	7.67	3.71	1.88	0.54	0.03	100.08	41.8	53.4	0.2
I-48-1	50.13	3.23	16.26	10.71	0.13	4.89	8.10	3.68	2.08	0.69	0.55	100.45	41.3	51.6	0.4
I-50-1	50.49	3.21	16.52	10.54	0.13	4.59	8.10	3.79	2.14	0.69	0.46	100.66	41.5	50.4	0.3
T9-2	50.36	3.09	16.63	10.51	0.14	4.87	8.08	3.73	2.09	0.68	0.59	99.59	41.8	52.0	0.3
Jin-2	52.14	2.60	16.78	10.20	0.13	4.70	7.28	4.05	2.26	0.52	0.51	100.16	42.9	51.8	0.4
Trachytes															
8-24-15	58.79	0.81	17.91	7.21	0.20	1.02	2.40	5.74	4.39	0.52	0.57	99.56	49.1	24.8	1.1
8-24-6	62.70	0.72	17.02	5.57	0.18	0.76	1.71	5.52	5.21	0.26	0.18	99.83	48.8	24.2	0.8
8-24-7	62.87	0.71	16.84	5.46	0.18	0.74	1.70	5.55	5.21	0.26	0.34	99.86	48.5	24.0	0.9
23	63.93	0.66	16.75	4.81	0.10	0.56	1.64	5.38	5.77	0.15	0.10	99.85	48.1	21.4	0.2
8-24-10	62.96	0.63	16.69	5.33	0.17	0.52	1.52	5.63	5.64	0.21	0.17	99.47	47.9	18.6	0.5
008-7	64.96	0.42	13.94	6.06	0.15	0.17	0.81	5.74	4.96	0.05	2.57	99.83	46.1	6.1	0.3
I-15-1	67.24	0.46	13.72	5.89	0.13	0.16	0.86	5.70	5.34	0.05	0.49	100.04	45.0	6.0	0.4
I-25-1	66.02	0.50	14.05	6.03	0.13	0.15	0.99	5.89	5.34	0.05	0.04	99.19	44.8	5.5	0.2
2-15-2	67.05	0.47	13.22	6.68	0.17	0.14	0.88	5.87	5.03	0.03	0.43	99.97	44.2	4.7	
2(1)S	66.68	0.37	13.10	6.18	0.15	0.12	0.80	6.11	5.26	0.02	0.63	99.42	43.2	4.3	0.6
I-7-2	67.55	0.43	13.33	6.01	0.14	0.08	0.86	6.02	5.10	0.02	0.12	99.66	43.9	3.0	0.1
I-8-1	67.95	0.43	13.44	5.89	0.14	0.06	0.78	5.89	5.17	0.02	0.31	100.08	44.6	2.3	
I-8-2	68.02	0.41	13.49	5.79	0.14	0.06	0.79	6.04	5.18	0.02	0.28	100.22	44.2	2.4	0.1
I-101-1	68.82	0.36	12.25	5.68	0.13	0.05	0.55	6.15	4.88	0.01	0.95	99.83	42.7	2.0	0.2

[a] The major elements data are from Chen (2013), representing weight percent (wt%).
[b] Total Iron as Fe_2O_3; Mg# = $Mg^{2+}/(Mg^{2+} + Fe^{2+})$, assuming $Fe^{3+}/(Fe^{2+} + Fe^{3+}) = 0.15$.
[c] CIA = Chemical Indexes of Alteration, defined as = molecular ratios of $Al_2O_3/(Al_2O_3 + CaO + Na_2O + K_2O) \times 100$ (Nesbitt and Young, 1982).
[d] The age of basalts and trachytes from Sun et al. (2008) and Chen (2013).

4. Results

4.1. Trace elements

Trace elements of the Changbaishan basalts and trachytes are presented in Table 2. The basalts are enriched in light rare earth elements (LREEs) relative to heavy rare earth elements and display OIB-like REE patterns (Fig. 2a). In the primitive mantle-normalized element spider diagram, these basalts show positive Ba, K and Pb, as well as negative U anomalies (Fig. 2b). In contrast, the trachytes also display enrichment in LREEs relative to heavy rare earth elements (Fig. 2c). And most of them have higher total REE abundances (158.3–225.2 ppm) than that of the OIB, as well as no or strong Eu anomaly ($\delta Eu = Eu_N/(Sm_N \times Gd_N)^{0.5}$ = 0.04–1.58, where subscript N denotes normalization to chondritic value (Sun and McDonough, 1989)) (Fig. 2c). Furthermore, the trachytes display weakly to extremely negative Sr, P and Ti anomalies, and weakly positive to negative Ba and Eu anomalies (Fig. 2d), probably reflecting significant minerals fractional crystallization.

4.2. Isotopic geochemistry

4.2.1. Sr and Nd isotopic compositions

Strontium and Nd isotopic data of the measured samples, as well as reference standard materials are presented in Table 3. The initial $^{87}Sr/^{86}Sr$ and $^{143}Nd/^{144}Nd$ ratios in the Changbaishan basalts and trachytes are corrected based on their ages (Wei et al., 2007; Sun et al., 2008) and Rb/Sr ratios, although they are very young. As a whole, the basalts have slightly enriched and limited variations in $^{87}Sr/^{86}Sr$ (0.70493–0.70506) and $^{143}Nd/^{144}Nd$ (0.512584–0.512619) ratios (Fig. 3), possibly reflecting the mixing trend between depleted mantle and EM-I component (Basu et al., 1991). In contrast, the trachytes have decoupled Sr—Nd isotopic compositions. They show a large $^{87}Sr/^{86}Sr$ range varying from 0.70490 to 0.71065, but display Changbaishan basalts-like $^{143}Nd/^{144}Nd$ ratios varying from 0.512584 to 0.512656 (Fig. 3).

4.2.2. Mg isotopic composition

Compared with the terrestrial mantle ($\delta^{26}Mg = -0.25 \pm 0.07$‰; Teng et al., 2010), Changbaishan basalts studied here have lower $\delta^{26}Mg$ and limited variation from −0.41 to −0.34‰ (Table 3). As shown in Fig. 4, these newly analyzed values are similar to the previously published data on Changbaishan basalts (−0.51 to −0.42‰) and most of < 110 Ma basalts from other parts of eastern China ($\delta^{26}Mg = -0.60$ to 0.23‰) reported by Yang et al. (2012), Huang et al. (2015), Tian et al. (2016), Li et al. (2017), Su et al. (2017), Sun et al. (2017) and Wang et al. (2017).

However, $\delta^{26}Mg$ in the trachytes varies between −0.27 and + 0.94‰ (Table 3). This exceeds the range measured for terrestrial igneous rocks or minerals reported thus far (Fig. 4). For example, their $\delta^{26}Mg$ values are heavier than I-, S- and A-type granitoids (−0.40 to +0.44‰, Shen et al., 2009; Li et al., 2010; Liu et al., 2010), syenites and syenogranites (−0.46 to −0.17‰, Ke et al., 2016). The most positive value is up to 1.1‰ heavier than those of the terrestrial mantle values ($\delta^{26}Mg = -0.25 \pm 0.07$‰, Teng et al., 2010) and 1.2‰ heavier than those of the underlying Changbaishan basalts (Fig. 4). Using previously published major and newly analyzed trace element and Sr—Nd data, we find that $\delta^{26}Mg$ inversely correlates with MgO, Al_2O_3, CaO, TiO_2, Sr (ppm), Nb/U and Zr/Hf values, but positively correlates with whole-rock SiO_2 and $^{87}Sr/^{86}Sr$ (Fig. 5).

5. Discussion

The chemical index of alteration (CIA) values for the Changbaishan basalts and trachytes vary from 40.8 to 44.0 and 42.7 to 49.1 (Table 1), within the range of un-weathered basalts (30–45) and granites and

Table 2
Trace element data for the alkali basalts and trachytes from Changbaishan, Northeast China.

Sample	T2-1	I-75-1	I-98-1	I-99-1	T2-5	I-55-1	I-34-1	I-47-1	I-48-1	I-50-1
Locality	Baishan				Laofangzixiaoshan		Heishigou			
Rock types	Basalts									
Trace elements (ppm)										
Li	10.4	7.6	7.7	8.2	7.3	7.2	8.3	8.4	6.9	6.7
Be	1.8	1.4	1.7	1.9	1.6	1.6	1.7	1.8	1.9	1.8
Sc	17.2	20.8	18.6	18.3	16.7	17.1	15.7	16.1	14.9	17.5
V	234.1	238.3	213.4	220.7	194.0	191.6	184.7	172.2	192.7	204.9
Cr	8.3	69.4	43.2	39.1	82.5	75.5	96.5	119.1	69.8	68.1
Co	41.4	37.6	34.1	35.6	39.8	37.0	43.8	42.1	34.8	36.0
Ni	38.2	37.1	37.9	33.8	60.8	46.6	91.8	87.9	45.9	40.5
Cu	35.2	46.1	38.9	41.1	39.1	32.5	32.2	37.0	34.4	39.3
Zn	166.1	154.7	149.6	153.7	152.7	150.8	150.5	145.2	133.4	141.9
Rb	42.4	40.9	36.5	39.0	35.1	32.9	31.7	33.2	35.6	37.7
Sr	642.9	750.1	655.0	670.8	681.9	663.9	623.7	636.5	854.9	790.5
Y	27.9	24.2	23.6	25.3	23.8	24.2	22.6	22.9	22.9	22.8
Zr	277.3	263.4	259.2	266.6	243.4	238.9	232.4	228.6	232.1	249.8
Nb	43.1	39.6	36.5	36.9	35.4	34.7	31.5	29.8	33.1	35.9
Cs	0.3	0.2	0.3	0.3	0.2	0.2	0.3	0.5	0.4	0.3
Ba	742.0	779.1	705.8	718.5	664.1	668.7	645.4	625.8	650.3	729.0
La	43.7	40.1	37.0	38.4	36.8	37.6	32.5	32.2	41.0	37.3
Ce	87.2	76.7	74.0	76.3	75.3	75.6	64.8	64.3	67.9	71.4
Pr	11.0	10.1	9.6	9.9	9.9	10.0	8.4	8.4	10.6	9.7
Nd	47.0	43.9	42.4	44.2	44.0	43.9	37.4	36.9	45.1	42.6
Sm	9.6	9.1	9.1	9.5	9.4	9.5	8.2	8.2	9.4	9.2
Eu	2.7	2.9	2.8	3.0	2.7	2.6	2.5	2.4	2.6	2.9
Gd	8.2	7.7	7.7	8.0	7.8	7.6	6.8	6.9	7.6	7.5
Tb	1.2	1.1	1.1	1.2	1.1	1.1	1.0	1.0	1.1	1.1
Dy	6.8	5.8	5.8	6.2	6.0	5.9	5.5	5.4	5.8	5.7
Ho	1.3	1.0	1.0	1.1	1.1	1.1	1.0	1.0	1.0	1.0
Er	3.1	2.4	2.4	2.6	2.6	2.5	2.4	2.5	2.4	2.4
Tm	0.4	0.3	0.3	0.3	0.3	0.3	0.3	0.3	0.3	0.3
Yb	2.5	1.8	1.9	2.0	2.0	2.0	1.9	2.0	1.8	1.9
Lu	0.4	0.3	0.3	0.3	0.3	0.3	0.3	0.3	0.3	0.3
Hf	7.1	6.5	6.5	6.8	6.0	5.8	5.8	5.6	5.6	6.0
Ta	2.8	2.6	2.3	2.4	2.2	2.2	2.0	1.9	2.1	2.2
Pb	5.8	4.8	4.9	5.0	4.8	5.0	4.6	4.6	4.8	4.5
Th	5.0	4.1	3.8	4.0	3.1	3.3	3.2	3.2	3.5	3.9
U	0.9	0.6	0.7	0.8	0.7	0.6	0.6	0.7	0.8	0.8
Ratios										
δEu^b	0.9	1.1	1.0	1.0	0.9	0.9	1.0	1.0	0.9	1.1
Nb/U	45.8	70.7	55.6	49.2	50.2	60.9	49.8	43.8	43.6	45.5
Zr/Hf	38.9	40.4	39.7	39.4	40.8	41.0	40.3	41.0	41.6	41.7

Sample	T9-2	Jin-2	8-24-15	8-24-6	8-24-7	8-24-10	23	008-7	I-15-1	I-25-1
Locality	Heishigou		Xiaobaishan				Baitoushan			
Rock types	Basalts		Trachytes							
Trace elements (ppm)										
Li	5.3	6.3	11.2	7.7	12.5	13.5	10.2	39.6	22.7	26.6
Be	1.3	1.3	2.9	2.7	3.2	3.4	4.7	9.1	5.0	5.6
Sc	15.2	12.5	4.5	7.9	8.5	9.9	5.5	4.2	4.4	5.1
V	162.8	134.9	5.6	6.7	6.6	3.7	10.1	4.2	2.1	1.7
Cr	72.1	85.3	5.0	3.7	3.3	3.7	4.7	6.7	1.9	1.4
Co	30.7	31.9	3.0	1.2	1.1	0.9	2.9	0.8	0.6	0.7
Ni	43.6	76.0	1.3	3.8	3.5	3.2	1.2	2.6	0.5	1.4
Cu	26.8	31.3	3.4	3.0	3.0	2.6	9.1	10.8	4.8	3.5
Zn	122.2	116.2	109.1	109.5	105.9	113.6	95.5	215.0	148.8	163.2
Rb	28.4	35.7	73.9	88.5	85.1	90.9	110.2	217.6	181.4	172.5
Sr	803.2	671.4	424.7	159.0	136.9	74.5	144.5	9.6	19.9	15.5
Y	19.0	19.3	32.0	30.1	29.9	30.2	34.2	65.4	41.0	48.2
Zr	215.6	209.4	604.8	444.9	453.1	481.8	604.7	1521.6	1158.3	943.0
Nb	32.1	29.1	70.9	51.6	52.6	53.4	69.6	133.9	128.0	104.1
Cs	0.1	0.2	1.1	0.8	0.8	0.9	1.2	2.8	0.6	0.6
Ba	685.0	677.0	1389.0	3422.6	3388.7	2434.4	485.7	17.7	82.2	51.1
La	32.6	31.2	69.0	57.9	56.1	57.7	52.8	109.2	84.9	81.0
Ce	64.5	61.0	103.3	106.7	86.9	100.5	92.9	208.7	216.9	164.5
Pr	8.4	7.7	15.3	13.7	12.9	13.3	12.1	23.4	20.2	19.3
Nd	35.8	32.9	56.6	52.2	49.3	50.4	45.7	86.1	76.3	74.6
Sm	7.5	7.0	9.1	8.8	8.4	8.7	8.7	15.7	14.1	14.5

(*continued on next page*)

Table 2 (*continued*)

Sample	T9-2	Jin-2	8-24-15	8-24-6	8-24-7	8-24-10	23	008-7	I-15-1	I-25-1
Locality	Heishigou		Xiaobaishan				Baitoushan			
Rock types	Basalts		Trachytes							
Eu	2.7	2.4	2.8	4.3	4.0	3.6	1.6	0.3	0.6	0.6
Gd	6.5	6.1	7.8	7.7	7.3	7.4	7.6	14.4	11.4	12.2
Tb	0.9	0.9	1.1	1.1	1.0	1.1	1.1	2.2	1.8	2.0
Dy	4.6	4.5	5.4	5.5	5.3	5.4	6.0	11.7	9.6	10.8
Ho	0.8	0.8	1.0	1.0	1.1	1.0	1.1	2.2	1.9	2.1
Er	1.9	1.9	2.8	2.6	2.7	2.7	3.0	5.7	4.8	5.4
Tm	0.3	0.3	0.4	0.4	0.4	0.4	0.4	0.8	0.7	0.8
Yb	1.5	1.5	2.5	2.4	2.4	2.4	2.6	4.9	4.7	4.9
Lu	0.2	0.2	0.4	0.4	0.4	0.4	0.4	0.7	0.7	0.8
Hf	5.4	5.3	12.0	9.1	9.3	9.9	12.6	29.3	29.4	23.7
Ta	2.1	1.9	3.9	2.6	2.6	2.7	3.5	7.0	8.7	7.1
Pb	4.4	4.6	7.5	10.0	9.8	7.7	6.2	16.8	17.1	16.3
Th	3.5	3.4	6.3	5.6	5.2	5.8	8.2	17.0	22.5	19.7
U	0.5	0.7	1.3	1.2	1.2	1.3	1.7	3.4	2.8	2.4
Ratios										
δEu[b]	1.2	1.1	1.0	1.6	1.6	0.58	1.37	0.06	0.15	0.13
Nb/U	64.7	42.5	54.5	41.5	43.7	41.7	42.2	39.4	46.2	43.6
Zr/Hf	39.8	39.6	50.4	48.8	48.7	48.8	47.9	51.9	39.4	39.7

Sample	2-15-2	2(1)S	I-7-2	I-8-1	I-8-2	I-101-1	GSR1	GSR1[a]	GSR3	GSR3[a]
Locality	Baitoushan						measuredd		measuredd	
Rock types	Trachytes									
Trace elements (ppm)										
Li	30.6	35.8	37.8	40.3	31.2	44.8	120.3	131.0	9.4	9.5
Be	5.3	9.0	6.8	6.0	6.7	13.3	13.1	12.4	2.4	2.5
Sc	4.5	3.2	3.7	4.8	3.8	3.5	6.2	6.1	16.6	15.2
V	8.4	0.5	1.9	0.4	0.9	0.3	22.3	24.0	160.1	167.0
Cr	2.9	1.4	2.8	3.9	1.7	1.2	2.3	5.0	127.1	134.0
Co	1.1	0.2	0.4	0.6	0.6	0.5	3.2	3.4	43.7	46.5
Ni	1.2	1.0	0.3	0.3	1.6	0.9	1.9	2.3	129.5	140.0
Cu	1.7	2.4	0.1	2.8	0.0	6.5	3.2	3.2	43.9	48.6
Zn	218.5	228.5	186.4	147.2	179.1	236.5	26.4	28.0	145.9	150.0
Rb	216.3	206.0	191.2	190.6	192.6	273.8	466.0	466.0	37.5	37.0
Sr	32.4	6.2	6.8	7.0	6.6	6.6	105.7	106.0	1063.1	1100.0
Y	44.6	89.8	22.8	39.3	26.5	98.5	60.1	62.0	20.9	22.0
Zr	1388.5	1313.1	1094.2	1087.6	1060.1	1942.7	159.2	167.0	261.3	277.0
Nb	154.6	159.6	124.5	121.3	119.7	183.3	39.1	40.0	68.7	68.0
Cs	1.1	1.5	1.2	0.8	1.1	4.1	39.6	38.4	0.5	0.5
Ba	100.9	6.1	9.4	11.1	9.1	8.1	334.6	343.0	552.4	526.0
La	87.1	171.1	106.1	87.9	85.8	187.9	53.4	54.0	57.5	56.0
Ce	174.9	289.9	214.8	224.5	177.6	348.6	104.3	108.0	106.4	105.0
Pr	21.9	36.5	22.7	21.4	18.8	38.8	12.6	12.7	13.2	13.2
Nd	83.5	140.8	84.8	81.1	70.0	146.7	45.7	47.0	55.2	54.0
Sm	15.2	26.9	13.6	15.5	12.1	27.3	9.4	9.7	10.7	10.2
Eu	0.5	0.3	0.3	0.4	0.3	0.5	0.9	0.9	3.2	3.2
Gd	12.2	22.7	9.5	12.5	9.4	24.0	9.1	9.3	9.1	8.5
Tb	1.9	3.7	1.3	1.9	1.4	3.9	1.6	1.7	1.2	1.2
Dy	10.3	20.5	6.7	10.5	7.1	22.2	9.9	10.2	5.8	5.6
Ho	2.0	4.0	1.3	1.9	1.3	4.4	2.1	2.1	1.0	0.9
Er	5.2	9.9	3.5	5.0	3.7	11.3	6.2	6.5	2.1	2.0
Tm	0.8	1.3	0.6	0.8	0.6	1.6	1.0	1.1	0.3	0.3
Yb	5.1	7.8	4.7	5.0	4.3	9.7	7.2	7.4	1.4	1.5
Lu	0.8	1.1	0.8	0.8	0.7	1.4	1.1	1.2	0.2	0.2
Hf	34.5	32.2	26.9	27.6	27.1	47.8	6.4	6.3	6.7	6.5
Ta	10.8	10.2	8.3	8.2	8.1	12.9	7.1	7.2	4.4	4.3
Pb	25.5	21.1	16.8	18.3	15.5	30.0	31.9	31.0	5.4	4.7
Th	29.1	28.5	20.0	22.9	21.9	38.4	52.1	54.0	7.3	6.0
U	2.2	4.5	3.7	3.0	3.4	7.5	19.1	18.8	1.6	1.4
Ratios										
δEu[b]	0.11	0.04	0.08	0.08	0.09	0.06				
Nb/U	70.3	35.3	33.7	41.0	35.3	24.6				
Zr/Hf	40.2	40.8	40.7	39.4	39.1	40.6				

[a] Reported values for the reference materials are from GeoREM (http://georem.mpch-mainz.gwdg.de).

[b] $\delta Eu = Eu_N/(Sm_N \times Gd_N)^{0.5}$, where subscript N denotes normalization to chondritic value (Sun and McDonough, 1989).

Table 3
Strontium, Nd and Mg isotopic compositions of the basalts and trachytes from Changbaishan area, Northeast China.

Sample	$\delta^{26}Mg$[a]	2SD[b]	$\delta^{25}Mg$	2SD	$\Delta^{25}Mg$[c]	$^{87}Sr/^{86}Sr$[d]	2σ	$^{143}Nd/^{144}Nd$[d]	2σ	ε_{Nd}
Basalts										
T2-1	−0.35	0.06	−0.18	0.05	0.01					
I-75-1	−0.39	0.07	−0.20	0.04	0.00	0.704937	0.000012	0.512619	0.000008	−0.37
I-98-1	−0.39	0.04	−0.17	0.04	0.03	0.704952	0.000013	0.512604	0.000012	−0.66
I-99-1	−0.39	0.08	−0.20	0.04	0.01	0.704929	0.000012	0.512611	0.000008	−0.53
T2-5	−0.41	0.07	−0.20	0.04	0.02	0.705016	0.000009	0.512604	0.000012	−0.66
I-55-1	−0.36	0.02	−0.22	0.08	−0.03	0.705043	0.000008	0.512584	0.000009	−1.05
I-34-1	−0.40	0.09	−0.21	0.03	0.00	0.705063	0.000011	0.512600	0.000008	−0.74
I-47-1	−0.38	0.05	−0.22	0.08	−0.02	0.705054	0.000013	0.512595	0.000009	−0.84
I-48-1	−0.38	0.05	−0.22	0.05	−0.02					
I-50-1	−0.39	0.07	−0.19	0.07	0.02					
T9-2	−0.34	0.09	−0.18	0.05	0.00	0.704980	0.000011	0.512600	0.000010	−0.74
Jin-2	−0.40	0.07	−0.21	0.05	0.00	0.705017	0.000011	0.512589	0.000011	−0.96
Trachytes										
8-24-15	−0.27	0.01	−0.13	0.02	0.01	0.704900	0.000008	0.512656	0.000009	0.35
Repeat a	−0.25	0.03	−0.13	0.03	0.00					
8-24-6	0.20	0.09	0.12	0.04	0.02	0.705231	0.000014	0.512624	0.000007	−0.27
Repeat a	0.19	0.06	0.11	0.05	0.01					
8-24-7	0.06	0.09	0.04	0.04	0.01	0.705169	0.000012	0.512623	0.000008	−0.29
Repeat a	0.11	0.02	0.06	0.03	0.00					
23	−0.09	0.07	−0.03	0.10	0.02	0.705013	0.000014	0.512605	0.000007	−0.64
Repeat a	−0.09	0.02	−0.04	0.03	0.00					
8-24-10	0.38	0.01	0.21	0.05	0.01	0.705242	0.000014	0.512630	0.000008	−0.16
Repeat a	0.37	0.05	0.21	0.06	0.02					
008-7	0.53	0.06	0.30	0.03	0.02	0.705892	0.000012	0.512602	0.000008	−0.70
Repeat a	0.47	0.04	0.23	0.02	−0.01					
I-15-1	0.31	0.03	0.17	0.05	0.01	0.704954	0.000014	0.512604	0.000008	−0.66
Repeat b	0.32	0.02	0.17	0.02	0.00					
Replicate	0.37	0.02	0.20	0.03	0.00					
I-25-1	0.32	0.07	0.18	0.04	0.01	0.705363	0.000011	0.512596	0.000011	−0.82
Repeat a	0.29	0.03	0.16	0.03	0.01					
2-15-2	0.03	0.06	0.02	0.04	0.01	0.705187	0.00001	0.512584	0.000009	−1.05
Repeat a	0.02	0.05	0.01	0.03	0.00					
2(1)S	0.84	0.05	0.44	0.02	0.00	0.710646	0.000014	0.512599	0.000008	−0.76
Repeat b	0.94	0.02	0.49	0.04	0.00					
Replicate	0.94	0.04	0.48	0.03	−0.01					
I-7-2	0.74	0.09	0.44	0.04	0.05	0.706437	0.000014	0.512600	0.000008	−0.74
Repeat b	0.69	0.05	0.37	0.06	0.02					
Replicate	0.74	0.02	0.40	0.03	0.01					
I-8-1	0.51	0.05	0.29	0.03	0.02	0.706811	0.000015	0.512596	0.000010	−0.82
Repeat a	0.40	0.04	0.22	0.05	0.01					
I-8-2	0.59	0.03	0.31	0.02	0.01	0.706458	0.000014	0.512595	0.000007	−0.84
Repeat b	0.68	0.04	0.36	0.05	0.01					
I-101-1	0.70	0.03	0.36	0.01	−0.01	0.706964	0.000015	0.512607	0.000009	−0.60
Repeat b	0.79	0.05	0.41	0.05	−0.01					
Standards										
BCR-2	−0.20	0.09	−0.10	0.03	0.00	0.705000	0.000014	0.512652	0.000008	
BHVO-2	−0.27	0.06	−0.12	0.10	0.02					
AGV-2	−0.17	0.02	−0.08	0.04	0.01					
Repeat b	−0.14	0.07	−0.06	0.02	0.01					
GSP-2	0.03	0.02	0.01	0.05	−0.01					
Repeat b	0.07	0.02	0.04	0.01	0.00					

[a] $\delta^{25,26}Mg = \{(^{25,26}Mg/^{24}Mg)_{sample}/(^{25,26}Mg/^{24}Mg)_{DSM3}-1) \times 1000$, DSM3 is a Mg solution made from pure Mg metal (Galy et al., 2003).
[b] 2SD = two times the standard deviation of the population of 4 repeat measurements of a sample solution.
[c] $\Delta^{25}Mg' = \delta^{25}Mg' - 0.521 \times \delta^{26}Mg'$,where $\delta^{25,26}Mg' = 1000 \times \ln[(\delta^{25,26}Mg + 1000)/1000]$ (Young and Galy, 2004).
[d] $^{87}Sr/^{86}Sr$ and $^{143}Nd/^{144}Nd$ are calculated based on their ages from Wei et al. (2007) and Sun et al. (2008). Repeat a: repeat sample dissolution and column chemistry (twice) of individual samples. Repeat b: repeat sample dissolution and column chemistry (three times) of individual samples. Replicate: repeat column chemistry (three times) and measurement for the same sample dissolution.

granodiorites (45–55) respectively, as noted by Nesbitt and Young (1982). This demonstrates the samples are not affected by surface alterations. We found the heaviest Mg isotopic composition ever reported in fresh igneous rocks also containing highly enriched $^{87}Sr/^{86}Sr$ but mantle source-like Nd isotopes, showing decoupled Mg—Sr and Nd isotopes signature. Below, we first discuss the source and petrogenesis of the trachytes and then assess the role of chemical weathering in the formation of trachytes on the basis of their decoupling of Mg—Sr and Nd isotopes. Finally, we evaluate their implications for the paleo-weathering of basaltic crust in NE China.

5.1. Source and petrogenesis of the Changbaishan trachytes

5.1.1. Source nature constrained by Changbaishan basalts

The Mg# (i.e. molar [MgO/(MgO + FeO)] × 100) of 37.6 to 53.4 in alkali basalts (Table 1), is lower than that of the normal MORB (~72; Langmuir et al., 1977), reflecting compositional evolution from their source. They have undergone olivine, pyroxene and plagioclase fractional crystallization based on photomicrographs (Chen, 2013) and rhyolite-MELTS simulations (Fig. 6). In addition, their OIB-like or even higher Nb/U (42.5–70.7) when compared with the continental crust (Rudnick and Gao, 2003) can rule out any contribution from crustal

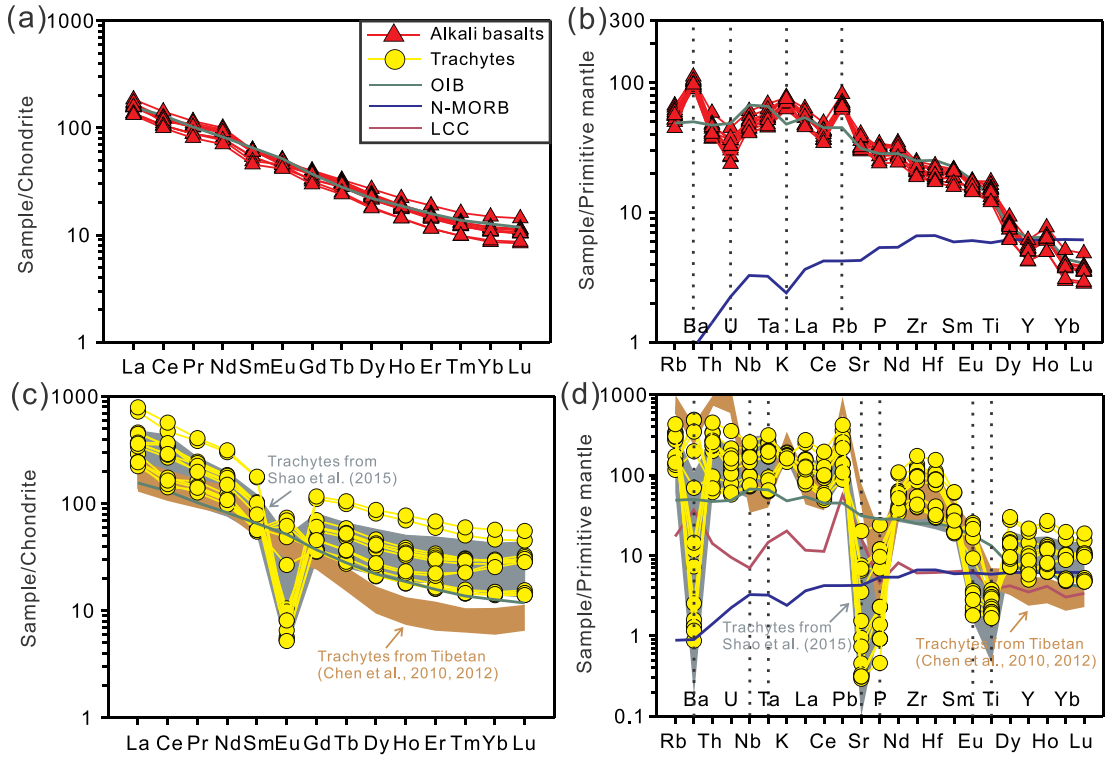

Fig. 2. Chondrite-normalized rare earth element (REE) diagram (a and c) and primitive mantle-normalized trace patterns (b and d) for the Changbaishan basalts and trachytes in this study. The primitive mantle and chondrite values are from Sun and McDonough (1989). Data source: OIB (ocean island basalt) and N-MORB (mid-ocean-ridge basalt) from Sun and McDonough (1989) and LCC (lower continental crust) is from Rudnick and Gao (2003). The colorful area represents trachytes from Tibetan (Chen et al., 2010, 2012) and southeast Queensland, Australia (Shao et al., 2015) for comparison.

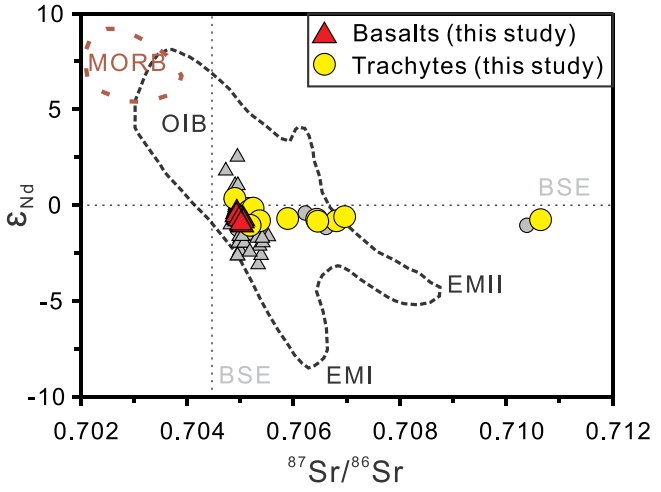

Fig. 3. $^{87}Sr/^{86}Sr$ vs. ε_{Nd} for the Changbaishan volcanic rocks. The grey triangle and circle represent the Changbaishan basalts and trachytes from literature, respectively. Data sources: isotopic endmember of the MORB and OIB are based on Zindler and Hart (1986). The compiled basalts and trachytes are from Xie et al. (1988), Fan et al. (2007), Zou et al. (2008), Kuritani et al. (2009), Guo et al. (2014, 2016) and Ma et al. (2015).

materials. Due to the limited Mg isotope fractionation (< 0.07‰ for $\delta^{26}Mg$) in basaltic differentiation (Teng et al., 2007, 2010) and the lack of any crustal contamination in the basalts, the low $\delta^{26}Mg$ signature must reflect some processes that occurred in the mantle source. This is also supported by the lack of any correlation between $\delta^{26}Mg$ and either SiO_2 or radiogenic Sr–Nd isotopes (Tables 1 and 3).

In addition, at least four different models have been proposed to interpret the enriched Sr-Nd-Pb isotopic signatures in Cenozoic basalts from NE China. (1) Metasomatism of ancient materials from mantle transition zone (Kuritani et al., 2011). (2) Enriched lithospheric mantle (Basu et al., 1991; Chen et al., 2007). (3) Influence from the subducted Pacific slab (Zhao et al., 2009) in the mantle transition zone (410–660 km). (4) Contribution from crustal materials (Zou et al., 2008). On the other hand, some previous studies suggest that the Cenozoic volcanic rocks originated from partial melting of the upwelling asthenosphere (e.g. Zou et al., 2003, 2008; Kuritani et al., 2011), while a few works considered that the dominated source are located within the SCLM (e.g. Basu et al., 1991; Chen et al., 2007).

In current work, the alkali basalts studied here have OIB-like rare earth elements (Fig. 2a), enrichment in LILEs (e.g. Ba, K and Pb) (Fig. 2b), low $\delta^{26}Mg$ and slightly high $^{87}Sr/^{86}Sr$ (0.70493–0.70506), similar to other basalts from the same volcanic area (e.g. Liu et al., 2015; Li et al., 2017). Here, we suggests that these characteristics of Changbaishan basalts probably reflect a similar origin as the < 110 Ma basalts from eastern China, which carried the fingerprint of subducted carbonates from Pacific slab (Li et al., 2017).

5.1.2. Relationship between basalts and trachytes

The Changbaishan trachytes are not the direct products of the mantle, because of their high SiO_2, low Mg# (2.0 to 24.8), as well as extremely low compatible Ni and Cr abundances (Table 2). Several lines of evidence strongly support that trachytes mainly formed by the protracted fractional crystallization of alkali basaltic magmas accompanied with some contamination. Firstly, field observations show that the trachytes are from a stratigraphic layer above the basalts and are less abundant than the Changbaishan basalts. Secondly, their trace element patterns (Fig. 2c and d) are clearly distinguishable from the Tibetan trachyte lavas that were interpreted to be originated from crust-derived melts (Chen et al., 2010, 2012). They do however display a high degree of similarity to the trachytes from southeast Queensland, Australia that formed by extensive fractional crystallization of basaltic melts (Shao

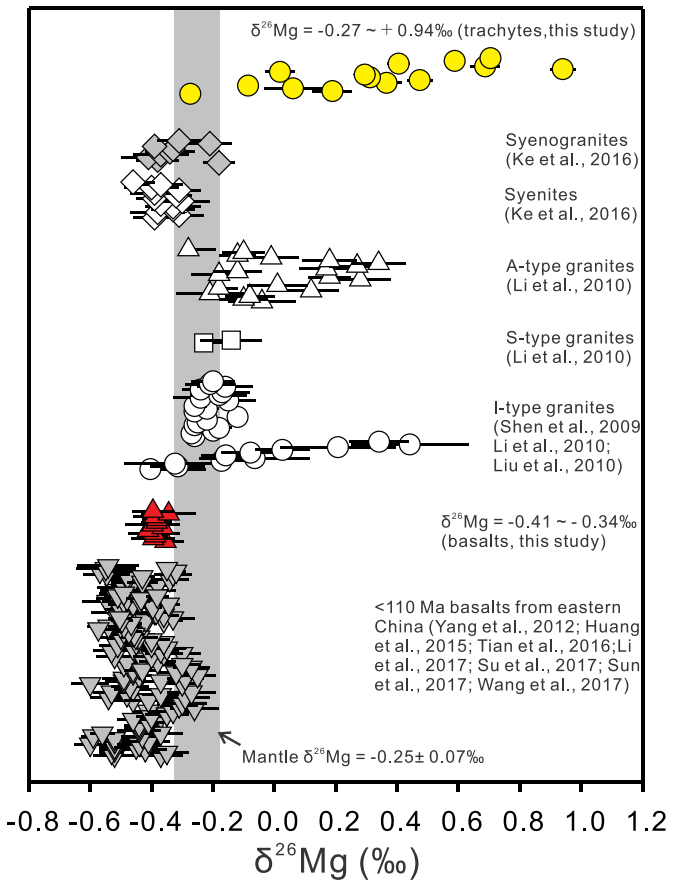
δ26Mg = -0.27 ~ + 0.94‰ (trachytes,this study)
Syenogranites (Ke et al., 2016)
Syenites (Ke et al., 2016)
A-type granites (Li et al., 2010)
S-type granites (Li et al., 2010)
I-type granites (Shen et al., 2009 Li et al., 2010; Liu et al., 2010)
δ26Mg = -0.41 ~ - 0.34‰ (basalts, this study)
<110 Ma basalts from eastern China (Yang et al., 2012; Huang et al., 2015; Tian et al., 2016;Li et al., 2017; Su et al., 2017; Sun et al., 2017; Wang et al., 2017)
Mantle δ26Mg = -0.25± 0.07‰
-0.8 -0.6 -0.4 -0.2 0.0 0.2 0.4 0.6 0.8 1.0 1.2
δ26Mg (‰)

Fig. 4. Magnesium isotopic compositions of volcanic rocks. Data source: < 110 Ma basalts from eastern China (Yang et al., 2012; Huang et al., 2015; Tian et al., 2016; Li et al., 2017; Su et al., 2017; Sun et al., 2017; Wang et al., 2017), granitoids rocks (Shen et al., 2009; Li et al., 2010; Liu et al., 2010), and syenites (Ke et al., 2016). The grey band is δ^{26}Mg range of the average Earth (−0.25 ± 0.07‰; Teng et al., 2010). Error bars on δ^{26}Mg represent 2 SD of repeated measurements and some error bars are smaller than symbols.

et al., 2015). Thirdly, phenocrysts of olivine, pyroxene and feldspar in basalts, trachytes and Holocene volcanic eruptions display continuous compositional evolution (Li et al., 2004). Finally, we use the rhyolite-MELTS software (Gualda et al., 2012; Ghiorso and Gualda, 2015) to model the fractional crystallization trend of the basaltic melts. As illustrated in Fig. 6, most of the major elements fall along the modelling curves, although the SiO_2 data is slightly high. This agrees well with previous studies (e.g. Xie et al., 1988; Liu et al., 1998, 2015; Li et al., 2004; Guo et al., 2015, 2016; Park et al., 2016).

However, given the highly variable $^{87}Sr/^{86}Sr$ (0.70490 to 0.71065) ratios in trachytes relative to that of the basalts, this characteristic may reflect the presence of crustal assimilation in the late magma evolution during the formation of trachytes. The following part will discuss the nature and evolution of the crustal material in detail.

5.2. Chemical weathering inducing decoupled Mg–Sr and Nd isotopes of trachytes

These trachytes display the highest δ^{26}Mg (up to 0.94 ± 0.04‰) among the previously reported data for fresh igneous rocks (Fig. 4). Interpretations of the largely variable δ^{26}Mg include thermal diffusion (Richter et al., 2009; Huang et al., 2010), fractional crystallization (Teng et al., 2007, 2010) and contribution of recycled crustal materials (Shen et al., 2009). We will attempt to evaluate these three mechanisms fractionating Mg isotopes in trachytes.

5.2.1. Thermal diffusion of Mg isotopes

Recent experimental studies suggested that thermal diffusion across a temperature gradient can induce fractionation in stable isotopes of Mg, Ca and Fe (e.g. Richter et al., 2009; Huang et al., 2010). For instance, heavy Mg isotopes, high MgO and low SiO_2 contents located at the cold end of a magmatic system along a temperature gradient (Richter et al., 2009) result in δ^{26}Mg positively varying with MgO and inversely varying with SiO_2 contents. However, δ^{26}Mg inversely correlates with MgO but positively correlates with SiO_2 observed in our trachyte samples (Fig. 5b and c), as well as the correlations with radiogenic isotopes (Sr and Nd; Fig. 5g) thus argue against thermal diffusion as causes for the highly variable Mg and Sr isotopic variations in the trachytes.

5.2.2. Effects of fractional crystallization on Mg isotopes of trachytes

Small Mg isotope fractionation has been observed for co-existing mantle olivine, clinopyroxene and orthopyroxene at high temperature in natural samples (Teng, 2017 and references therein). Indeed, during magma differentiation, the residual melt should enrich heavier Mg isotopes when compared with the olivine, pyroxene and ilmenite, given that Mg is in six-fold and five-fold coordination in olivine-pyroxene-ilmenite and silicate melts (Wilding et al., 2004; Henderson et al., 2006).

Here, we adopt the fractional crystallization model to explore Mg isotopic variation using the results from rhyolite-MELTS simulation. The fractionation factors (i.e. isotopic difference between mineral and melt) are obtained by experiments and studies on natural samples. Five constant fractionation factors of $\delta^{26}Mg_{olivine\text{-}melt} = -0.07‰$ (Teng et al., 2007), $\delta^{26}Mg_{cpx\text{-}melt} = -0.04‰$, $\delta^{26}Mg_{opx\text{-}melt} = -0.05‰$ (deducted from Huang et al., 2013), $\delta^{26}Mg_{ilmenite\text{-}melt} = -0.32‰$ (Chen et al., 2018) and $\delta^{26}Mg_{spinel\text{-}melt} = +0.22‰$ (Liu et al., 2011; Xiao et al., 2013) are assumed in this model.

As shown in Fig. 7, our results indicate that fractional crystallization of the basaltic melts with a starting component of MgO = 8.2 wt% and δ^{26}Mg = −0.38‰ will make δ^{26}Mg remaining in the melt increase up to approximately +0.05‰, when MgO decreases as low as 0.05 wt% (Fig. 7). Notably, this value still cannot account for most of the δ^{26}Mg in trachyte rocks. Hence, the isotope offset between alkali basalts and trachytes (up to 1.2‰) is too large to be explained by a single fractional crystallization process. Therefore, although fractional crystallization process has slightly elevated the δ^{26}Mg in trachytes, it is not the main mechanism that highly fractionated the Mg isotopes.

5.2.3. The assimilation and fractional crystallization (AFC) model

From the above discussion, crustal materials are required in this volcanic system. However, the decoupling of Mg–Sr and Nd isotopes in trachytes rule out the assimilation of common silicate materials. Because input of ancient or young crustal rocks (i.e. the underlying Archean-Proterozoic basement rocks) would have resulted in coupled Sr–Nd isotopic variation. Considering the correlations between δ^{26}Mg and both the major and trace element variations and $^{87}Sr/^{86}Sr$ ratios (Fig. 5), at least one component is needed to produce the high δ^{26}Mg values in Changbaishan trachytes, which is characterized by heavy δ^{26}Mg (> +0.94‰), high $^{87}Sr/^{86}Sr$ (> 0.7110), basalts-like $^{143}Nd/^{144}Nd$ (~0.512600), low MgO, Nb/U and Zr/Hf ratios. It has been reported that the continental crustal rocks (including TTG gneisses, granulites, I-, S- and A-type granites, syenites and syenogranites) yield a large δ^{26}Mg variation of −0.76 to +0.44‰ (Shen et al., 2009; Li et al., 2010; Liu et al., 2010; Teng et al., 2013; Ke et al., 2016; Yang et al., 2016). However, they are still lower than the heaviest value (+0.94‰) recorded in trachytic rocks. In contrast, although the supracrustal materials show larger Mg isotopic variations, e.g. pelites (−0.52 to +0.92‰; Li et al., 2010), shales (−0.27 to +0.49‰; Li et al., 2010), and mudrocks (−0.17 to +0.25‰; Wang et al., 2015), they are still not the appropriate candidates. To date, continental weathering of the diabase and basalts produce extremely variable

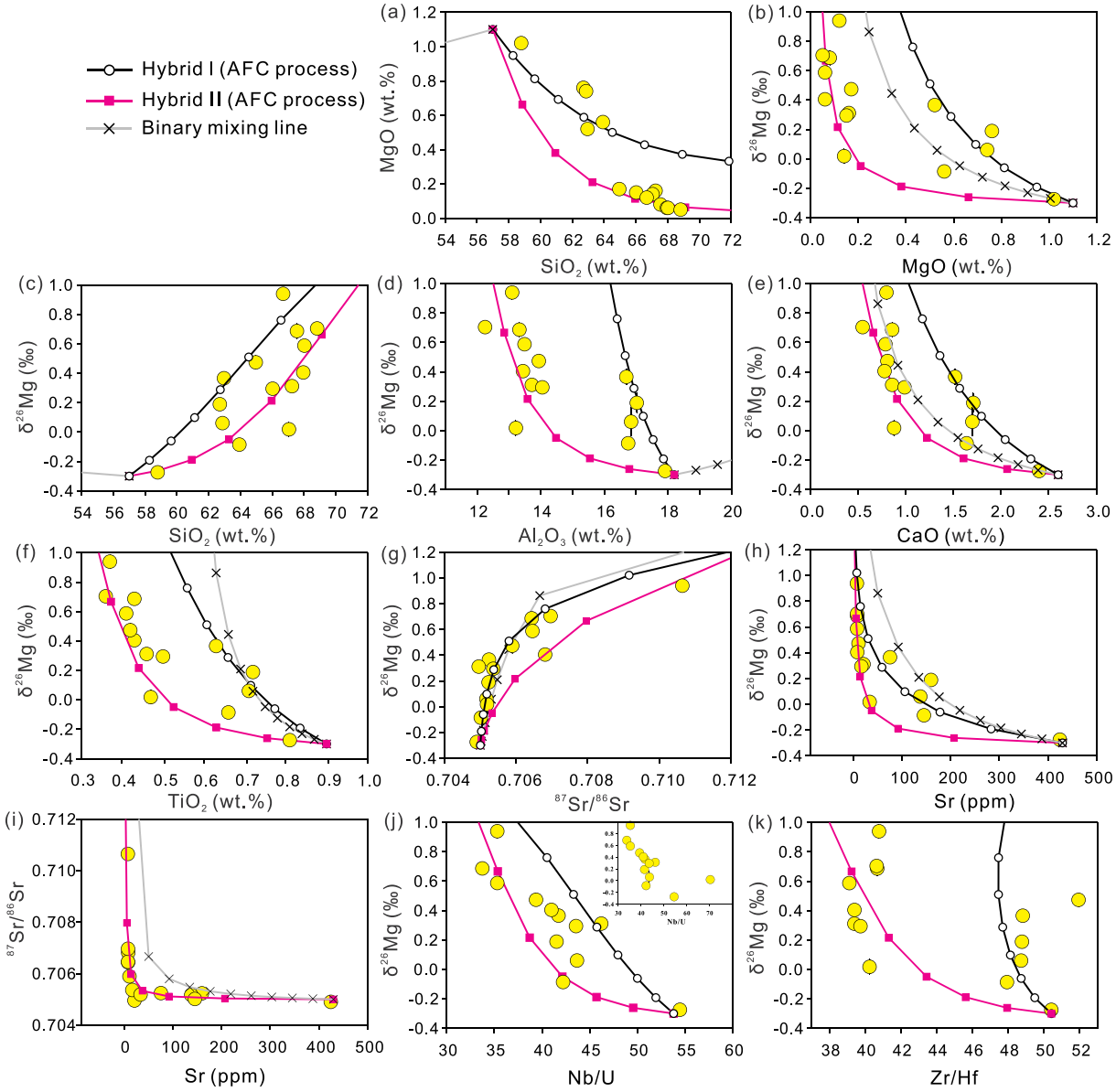

Fig. 5. Geochemical data on Changbaishan basalts and trachytes samples. (a) SiO_2 versus MgO. (b) $\delta^{26}Mg$ versus MgO. (c) $\delta^{26}Mg$ versus SiO_2. (d) $\delta^{26}Mg$ versus Al_2O_3. (e) $\delta^{26}Mg$ versus CaO. (f) $\delta^{26}Mg$ versus TiO_2. (g) $\delta^{26}Mg$ versus $^{87}Sr/^{86}Sr$. (h) $\delta^{26}Mg$ versus Sr (ppm). (i) $^{87}Sr/^{86}Sr$ versus Sr (ppm). (j) $\delta^{26}Mg$ versus Nb/U and (k) $\delta^{26}Mg$ versus Zr/Hf. Most of the error bars associated with an individual data is within the size of the symbol. Grey line with black cross represents binary mixing line between the initial magma endmember and continental weathered residue, characterized by heavy $\delta^{26}Mg$, low SiO_2 (wt%), MgO (wt%), CaO (wt%) and TiO_2 (wt%) and high Al_2O_3 (wt%). The two colored curves represent two different "hybrid" models describing evolution of a magma chamber formed by mixing of initial magma and weathered residue and simultaneously undergoing fractional crystallization (AFC; Depaolo, 1981). For these calculations, the initial magma chamber was assumed to be similar to the geochemical characteristics of sample 8–24-15. Two different endmembers of weathered residue were employed based on the Mg isotopic, major and trace element variations (Ma et al., 2007, 2010; Ma, 2011; Huang et al., 2012; Liu et al., 2013, 2014). Circles on the curves represent 10% AFC increments. The modelled parameters are listed in Table 4.

$\delta^{26}Mg$ varying from −0.49‰ to +1.81‰ (Teng, 2017 and references therein), which can cover the largest value of +0.94‰ in trachytes. Furthermore, previous studies suggested that the Cenozoic basalts during intense weathering could induce apparent $^{87}Sr/^{86}Sr$ fractionation, but limited influence on Nd isotopes (Ma et al., 2010; Ma, 2011). This can be attributed to differential decomposition of minerals containing heterogeneous $^{87}Sr/^{86}Sr$ ratios (Blum and Erel, 1995; Negrel, 2006) or input of extraneous Sr with high $^{87}Sr/^{86}Sr$ ratios from aeolian deposits or groundwater (Price et al., 1991; Stewart et al., 2001; Kurtz et al., 2001; Dia et al., 2006; Ma et al., 2010). Additionally, the unique structure of the Changbaishan shield basalts provides favorable conditions for the formation of weathering basalts. Thus, the early-forming basalts that experienced intense weathering would be covered by the late fresh basalts that eventually formed a volcano with a layered structure. This explanation agrees well with a recent study of high $\delta^{18}O$ (3.68–5.03‰) in zircons from the trachytes, indicating the occurrence of altered rocks in the shallow magma chamber beneath the Changbaishan volcanic area (Cheong et al., 2017). Thus, the weathered basalts recycling into the trachytic magma chamber provide a reasonable and feasible explanation of the data.

Here, we adopt the AFC equation (Depaolo, 1981) to model the $\delta^{26}Mg$ versus major and trace elements and $^{87}Sr/^{86}Sr$ variations using reasonable parameters (Table 4) on the basis of residue of weathered basalts. As shown in Fig. 5, the simple binary mixing between the initial component and preexisting residue of weathered basalts is unlikely to match most of the major elemental variations. For example, the major

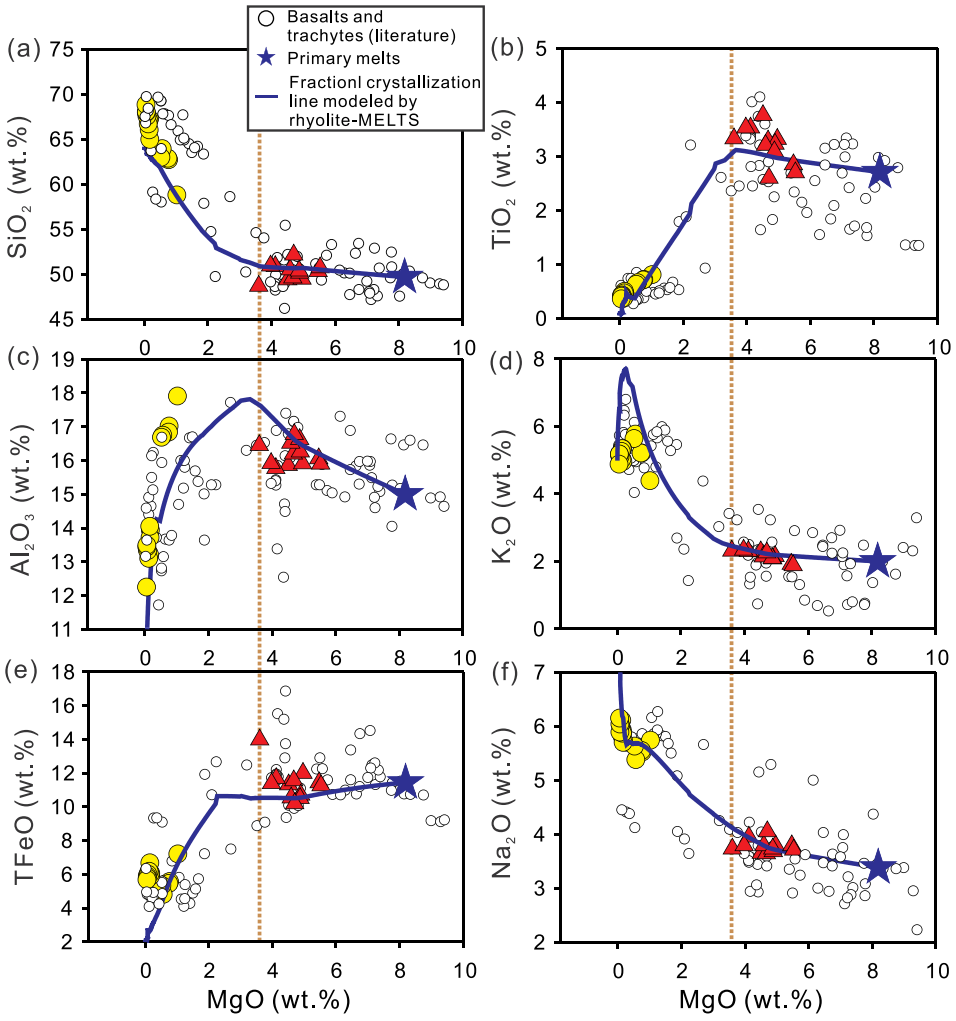

Fig. 6. Major oxide variations of the Changbaishan volcanic rocks. The white circles represent Changbaishan basalts and trachytes from literatures (Xie et al., 1988; Hsu et al., 2000; Fan et al., 2006; Chen et al., 2007; Zou et al., 2008; Chen, 2013; Guo et al., 2014; Ma et al., 2015). The blue curves represent the fractional crystallization (e.g., olivine, pyroxene, ilmenite) processes modelled using rhyolite-MELTS software (Gualda et al., 2012; Ghiorso and Gualda, 2015). The primary melts of SiO_2 (49.7 wt%), TiO_2 (2.7 wt%), Al_2O_3 (15.0 wt%), Fe_2O_3 (1.1 wt%), FeO (9.3 wt%), MnO (0.15 wt%), MgO (8.2 wt%), CaO (7.4 wt %), Na_2O (3.4 wt%), K_2O (2.0 wt%), P_2O_5 (0.4 wt%) and H_2O (0.6 wt%) is based on a large number of simulations. The given conditions are ~4.2 kbar and oxygen fugacity (ΔQFM-1). The evolution line represents the temperature decrements. The right part separated by the dash orange line is basaltic composition and the left part is intermediate-felsic composition. (For interpretation of the references to color in this figure legend, the reader is referred to the web version of this article.)

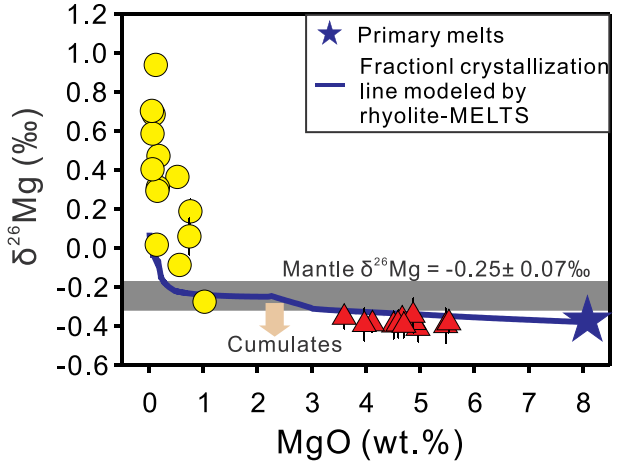

Fig. 7. Modelling the evolution of $\delta^{26}Mg$ during crystallization from the parental magma by removal of mafic minerals (olivine, clinopyroxene, spinel and ilmenite) based on the rhyolite-MELTS output result. Here, we adopted the fractional crystallization equation to model the $\delta^{26}Mg$ variation. The amount of fractional crystallization of each mineral is in accordance with the predicted results from rhyolite-MELTS. The blue line is the evolutionary trend of Mg isotopes. Some error bars on $\delta^{26}Mg$ are smaller than symbols. (For interpretation of the references to color in this figure legend, the reader is referred to the web version of this article.)

elements Fe_2O_3 and Al_2O_3 will be increasing, whereas SiO_2, MgO, Na_2O, K_2O and CaO dramatically decrease in the weathered residual when compared with their parent rocks (e.g. Ma et al., 2007; Liu et al., 2013). Binary mixing between the initial component and weathered products will elevate Fe_2O_3 and Al_2O_3 content, but lower the SiO_2, MgO and CaO concentrations. However, correlations between $\delta^{26}Mg$ and both the SiO_2 and Al_2O_3 contents in the trachytes show opposing binary mixing trend lines (Fig. 5c and d). Furthermore, although some elements can be modelled by binary mixing, an unrealistically high proportion of weathered materials (> 70%) is required to fully fit $\delta^{26}Mg$ variations in the trachyte lavas (Fig. 5b and e-h).

The AFC model in contrast treats Mg as a compatible element with a partition coefficient $D_{Mg} > 1$. Silicon is incompatible with $D_{Si} < 1$ in the fractional assemblages. Thus, Mg is rapidly depleted from the magma whilst Si gradually increases. In this case, two weathered end-member products are required to fit the trachyte variations falling on the AFC calculation curves (Fig. 5). This result shows that up to 50% AFC can reach the Mg—Sr isotopes and other elemental variations. That may be ascribed to the much lower volume of trachytes relative to the shield basalts, so that minor volume of intensely weathered products can easily reach this proportion. Therefore, the AFC process associated with the weathered basalts most likely resulted in the decoupled Mg—Sr and Nd isotopes, accompanied by major- and trace elemental variations in trachytes.

Table 4
Summarized parameters for model calculations.

Endmembers	$\delta^{26}Mg$	MgO	D_{Mg}	SiO_2	D_{Si}	Al_2O_3	D_{Al}	CaO	D_{Ca}	TiO_2	D_{Ti}	$^{87}Sr/^{86}Sr$	Sr	D_{Sr}	Nb	D_{Nb}	U	D_U	Zr	D_{Zr}	Hf	D_{Hf}
Primary melt	−0.3	1.1		57		18.2		2.6		0.9		0.705000	430		71		1.32		605		12	
Assimilant 1	1.8	0.15	3	20	0.52	25	1.6	0.5	1.7	0.6	1.7	0.718000	7	4	38.2	0.39	1.25	0.18	207	0.31	8.78	0.25
Assimilant 2	1.5	0.6	1.5	34	0.69	22	1.2	1.2	1.3	0.6	1.2	0.715000	10	2.5	52.4	0.39	0.87	0.18	285	0.25	10	0.33

These parameters were adopted in the AFC model (Fig. 5). The unit of the major oxides (MgO, SiO_2, Al_2O_3, CaO and TiO_2) is weight percent (wt%) and unit of trace elements (Sr, Nb, U, Zr and Hf) is ppm. The abundance of major and trace elements as well as $\delta^{26}Mg$ of the assimilant 1 and 2 are based on the studies of weathered silicate profiles (Ma et al., 2007, 2010; Ma, 2011; Huang et al., 2012; Liu et al., 2013, 2014).

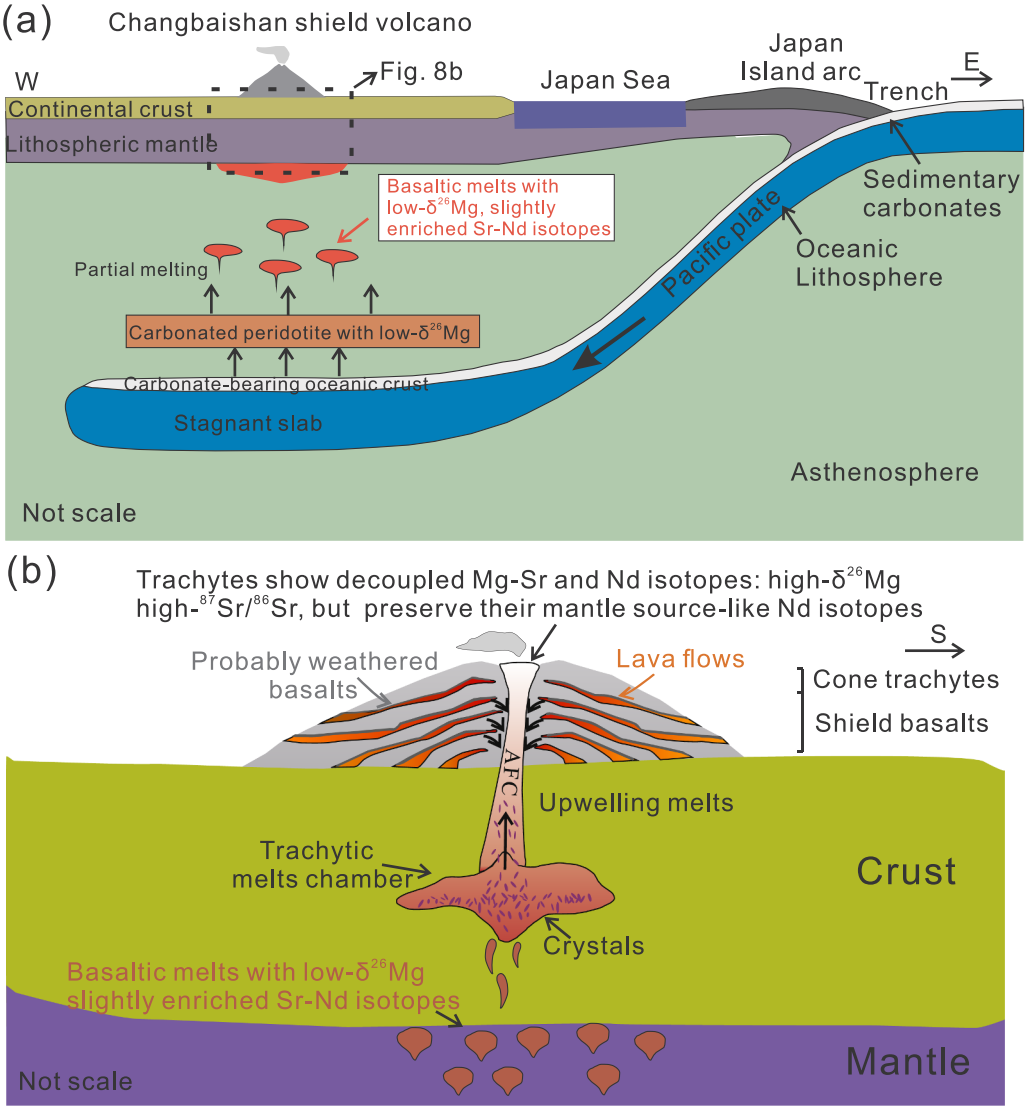

Fig. 8. A cartoon model illustrating the origin of the Changbaishan basalts and trachytes. (a) A subducted Pacific stagnant slab existed in the mantle transition zone underneath eastern China (modified from Huang and Zhao, 2006). This plate brought sedimentary carbonates with low $\delta^{26}Mg$ into the asthenosphere and formed carbonated peridotites that can generate basaltic melts with low $\delta^{26}Mg$ (e.g. Li et al., 2017). (b) A part of the basaltic melts with low-$\delta^{26}Mg$ values upwelled and entered into the magma chamber in the crust. Then, this melt continued to rise through the magmatic channel and involved of some weathered basalts residue (characterized by extreme high $\delta^{26}Mg$ and enriched $^{87}Sr/^{86}Sr$ ratios) via AFC processes. At last, the late erupted trachytes obtain heavy Mg and enriched Sr isotopes but preserved their original Nd isotopes compared to their source melts (Figs. 4, 5).

5.3. Approach to trace the paleo-weathering of basaltic crust in Earth's surface

Our study of the trachytes clearly show remarkable decoupling of Mg–Sr and Nd isotopes, as well as enriched Mg–Sr isotopic compositions relative to their primary sources (Figs. 4 and 5). This finding probably has the implication to reconstruct the Earth's climate system by using natural records of past climate change coupled with theoretical models. In combination with the major and trace element variations, these characteristics strongly point to the existence of intensely-weathered residue of basalts in the volcano shield. This extremely chemical weathering requires strong precipitation, wind or high temperature conditions. Additionally, based on previous studies of weathered basalts from South China (Ma et al., 2007; Huang et al., 2012) and Columbia River (Liu et al., 2014), we speculate that ~4–5 Mys continued weathering may be required to generate such a high degree of weathering ($\delta^{26}Mg$ up to +1.8‰). Based on K–Ar dating and field observations (Zhang et al., 2018 and references therein), basalts distributed in Changbaishan area mainly included the early pre-shield basalts with the age of ~22.6 to 10.4 Ma, and the late shield basalts with the age of ~5.02 to 1.05 Ma. Hence, it is likely that the pre-shield basalts would be intensely weathered during the long time span of the pre-shield stage (~12 Mys), the interval of pre-shield stage and the shield-forming stage (~5 Mys), and during the shield-forming stage (~4 Mys). An early work by Zou et al. (2004) proposed hot and humid conditions (with annual average temperature of > 19 °C and the annual

rainfall of > 165 cm) existed in SE China during 17–15 Ma, based on Sr–Nd isotope systematics of xenoliths in SE China basalts at Fujian. Their interpretation was supported by subsequent studies (Kurschner et al., 2008; Jiang and Ding, 2008). In addition, because of the expansion of the eastern Antarctica ice sheet during the middle Miocene and the formation of the Greenland ice sheet in the late Miocene (Larsen et al., 1994; Zachos et al., 2001), global temperature gradually cooled since ~15 Ma. Taking the above two factors into account, we suggested that there probably existed a warm and humid condition in NE China during 17–15 Ma, which induced intense chemical weathering for pre-shield basalts. Subsequently, they were also affected by weakened weathering until the end of Miocene. This ancient weathered basaltic crust would be covered by the late fresh volcanic flow during Pliocene and became a part of the volcanic cone. As the basalt continued to erupt, the volcanic cone increased and grew, and the magma chamber also rose. When this melt rose to the surface, it would assimilate the ancient weathered crust in the volcanic cone. Finally, the latest formed trachytes from the volcano cone can obtain this weathering signature through AFC processes when they passed through the magma vent (Fig. 8). That is ascribed to two aspects (1) the very low abundant (< 5%) of trachytes accounts for the total basalts (Jin and Zhang, 1994) and (2) the relatively low upwelling rate and long store time for the intermediate-felsic magma in the crustal chamber. The trachytes can obtain higher Mg and Sr isotopes through the AFC processes. Hence, our results suggest that the Northeast Asia once had a warm and humid climate during the middle Miocene.

This study provides a specific case that systematic studies of Sr-Nd-Mg isotopes, and conventional elements on late stage volcanic rocks can provide a potentially efficient way to explore the paleo-weathered basaltic crust.

6. Conclusions

We present high-precision Sr-Nd-Mg isotopes, as well as trace elemental abundance on a suite of early erupted basalts and late trachytes from Changbaishan stratovolcano, NE China. Combined with previous studies, alkali basalts have lower δ^{26}Mg (−0.51 to −0.34‰) than that of the mantle, but similar to most of the late Cretaceous and Cenozoic basalts from eastern China (δ^{26}Mg = −0.60 to −0.23‰). These basalts have the same origins with recycled carbonates metasomatism as the < 110 Ma basalts from other eastern China. In contrast, the trachytes show decoupled Mg–Sr and Nd isotopes, i.e. largely variable δ^{26}Mg values from −0.27 up to +0.94‰, high $^{87}Sr/^{86}Sr$ (0.70490 to 0.71065), but mantle source-like $^{143}Nd/^{144}Nd$ (0.512584 to 0.512656). Their decoupled Sr-Nd-Mg isotopes cannot be explained by thermal diffusion, fractional crystallization or simple crustal contamination processes. Instead, based on the correlations between δ^{26}Mg and $^{87}Sr/^{86}Sr$, trace elemental ratios (e.g. Nb/U and Zr/Hf) and major oxides (e.g. MgO, SiO_2, CaO), they are suggested to reflect the role of chemical weathering residue. These observations together strongly support the existence of paleo-weathered crusts in Changbaishan volcanic cone. Combined with the paleo-environmental evidence, intense chemical weathering probably took place during the middle Miocene period. Collectively, coupled Sr-Nd-Mg isotopes and conventional major and trace elements on late stage volcanic rocks in this study provides a potentially efficient way to explore the existence of paleo-weathered crusts. This study shed new light on the research on paleo-weathered crust.

Acknowledgements

We would like to thank the associate editor Anthony Dosseto, Prof. Hai-Bo Zou and one anonymous reviewer for their insightful comments, which greatly improved the manuscript. Bing-Yu Gao and Wen-Jun Li are thanked for assistance in trace elements analyses and Chao-Feng Li for assistance in Sr and Nd isotopic analyses at IGGCAS. We also thank Hitesh Changela and Xin-Yang Chen for insight and detailed comments. This work was supported by the Strategic Priority Research Program of the Chinese Academy of Sciences (Grant number XDB18000000), National Natural Science Foundation of China (Grants number 41730214), National Postdoctoral Program (2018M631566) and National Postdoctoral Program for Innovative Talents (BX201700237) to Heng-Ci Tian.

References

An, Y.J., Wu, F., Xiang, Y.X., Nan, X.Y., Yu, X., Yang, J.H., Yu, H.M., Xie, L.W., Huang, F., 2014. High-precision Mg isotope analyses of low-Mg rocks by MC-ICP-MS. Chem. Geol. 390, 9–21.

Balagizi, C.M., Darchambeau, F., Bouillon, S., Yalire, M.M., Lambert, T., Borges, A.V., 2015. River geochemistry, chemical weathering, and atmospheric CO_2 consumption rates in the Virunga Volcanic Province (East Africa). Geochem. Geophys. Geosyst. 16, 2637–2660.

Basu, A.R., Wang, J.W., Huang, W.K., Xie, G.H., Tatsumoto, M., 1991. Major Element, Ree, and Pb, Nd and Sr isotopic geochemistry of cenozoic volcanic rocks of Eastern China: implications for their origin from suboceanic-type mantle reservoirs. Earth Planet. Sci. Lett. 105, 149–169.

Berner, R.A., Lasaga, A.C., Garrels, R.M., 1983. The carbonate-silicate geochemical cycle and its effect on atmospheric carbon dioxide over the past 100 millions years. Am. J. Sci. 284, 641–683.

Blum, J.D., Erel, Y., 1995. A silicate weathering mechanism linking increases in marine $^{87}Sr/^{86}Sr$ with global glaciation. Nature 373, 415–418.

Bryan, S.E., Ernst, R.E., 2008. Revised definition of large igneous provinces (LIPs). Earth Sci. Rev. 86, 175–202.

Chen, X.W., 2013. Crystallization Differentiation and Magma Mixing Process of the Tianchi Volcano, Changbaishan. Master Thesis. Institute of Geology, China Earthquake Administration, Beijing, pp. 1–121 (in Chinese).

Chen, Y., Zhang, Y.X., Graham, D., Su, S.G., Deng, J.F., 2007. Geochemistry of Cenozoic basalts and mantle xenoliths in Northeast China. Lithos 96, 108–126.

Chen, J.L., Xu, J.F., Wang, B.D., Kang, Z.Q., Jie, L., 2010. Origin of Cenozoic alkaline potassic volcanic rocks at KonglongXiang, Lhasa terrane, Tibetan Plateau: products of partial melting of a mafic lower-crustal source? Chem. Geol. 273, 286–299.

Chen, J.L., Zha, W.X., Xu, J.F., Wang, B.D., Kang, Z.Q., 2012. Geochemistry of Miocene trachytes in Bugasi, Lhasa block, Tibetan Plateau: mixing products between mantle- and crust-derived melts? Gondwana Res. 21, 112–122.

Chen, L.M., Teng, F.-Z., Song, X.Y., Hu, R.Z., Yu, S.Y., Zhu, D., Kang, J., 2018. Magnesium isotopic evidence for chemical disequilibrium among cumulus minerals in layered mafic intrusion. Earth Planet. Sci. Lett. 487, 74–83.

Cheong, A.C.S., Sohn, Y.K., Jeong, Y.J., Jo, H.J., Park, K.H., Lee, Y.S., Li, X.H., 2017. Latest Pleistocene crustal cannibalization at Baekdusan (Changbaishan) as traced by oxygen isotopes of zircon from the Millennium Eruption. Lithos 284, 132–137.

Choi, H.O., Choi, S.H., Schiano, P., Cho, M., Cluzel, N., Devidal, J.-L., Ha, K., 2017. Geochemistry of olivine-hosted melt inclusions in the Baekdusan (Changbaishan) basalts: implications for recycling of oceanic crustal materials into the mantle source. Lithos 284-285, 194–206.

Chung, S.L., Jahn, B.M., 1995. Plume-Lithosphere Interaction in Generation of the Emeishan Flood Basalts at the Permian-Triassic Boundary. Geology 23, 889–892.

Depaolo, D.J., 1981. Trace-element and isotopic effects of combined wallrock assimilation and fractional crystallization. Earth Planet. Sci. Lett. 53, 189–202.

Dessert, C., Dupré, B., Francois, L.M., Schott, J., Gaillardet, J., Chakrapani, G.J., Bajpai, S., 2001. Erosion of Deccan Traps determined by river geochemistry: impact on the global climate and the $^{87}Sr/^{86}Sr$ ratio of seawater. Earth Planet. Sci. Lett. 188, 459–474.

Dessert, C., Dupré, B., Gaillardet, J., Francois, L.M., Allegre, C.J., 2003. Basalt weathering laws and the impact of basalt weathering on the global carbon cycle. Chem. Geol. 202, 257–273.

Dessert, C., Lajeunesse, E., Lloret, E., Clergue, C., Crispi, O., Gorge, C., Quidelleur, X., 2015. Controls on chemical weathering on a mountainous volcanic tropical island: Guadeloupe (French West Indies). Geochim. Cosmochim. Acta 171, 216–237.

Dia, A., Chauvel, C., Bulourde, M., Gerard, M., 2006. Eolian contribution to soils on Mount Cameroon: isotopic and trace element records. Chem. Geol. 226, 232–252.

Dufek, J., Bachmann, O., 2010. Quantum magmatism: magmatic compositional gaps generated by melt-crystal dynamics. Geology 38, 687–690.

Fan, Q.C., Sui, J.L., Wang, T.H., Li, N., Sun, Q., 2006. Eruption history and magma evolution of the trachybasalt in the Tianchi volcano, Changbaishan. Acta Petrol. Sin. 22, 1449–1457 (in Chinese).

Fan, Q.C., Sui, J.L., Wang, T.H., Li, N., Sun, Q., 2007. History of volcanic activity, magma evolution and eruptive mechanisms of the Changbai volcanic province. Geol. J. China Univ. 13, 175–190 (in Chinese).

Gaillardet, J., Dupré, B., Louvat, P., Allegre, C.J., 1999. Global silicate weathering and CO_2 consumption rates deduced from the chemistry of large rivers. Chem. Geol. 159, 3–30.

Galy, A., Yoffe, O., Janney, P.E., Williams, R.W., Cloquet, C., Alard, O., Halicz, L., Wadhwa, M., Hutcheon, I.D., Ramon, E., Carignan, J., 2003. Magnesium isotope heterogeneity of the isotopic standard SRM980 and new reference materials for magnesium-isotope-ratio measurements. J. Anal. At. Spectrom. 18, 1352–1356.

Ghiorso, M.S., Gualda, G.A.R., 2015. An H_2O-CO_2 mixed fluid saturation model compatible with rhyolite-MELTS. Contrib. Mineral. Petrol. 169.

Gualda, G.A.R., Ghiorso, M.S., Lemons, R.V., Carley, T.L., 2012. Rhyolite-MELTS: a

Modified Calibration of MELTS Optimized for Silica-rich, Fluid-bearing Magmatic Systems. J. Petrol. 53, 875–890.
Guo, W.F., Liu, J.Q., Guo, Z.F., 2014. Temporal variations and petrogenetic implications in Changbai basaltic rocks since the Pliocene. Acta Petrol. Sin. 30, 3595–3611 (in Chinese).
Guo, W.F., Liu, J.Q., Xu, W.G., Li, W., Lei, M., 2015. Reassessment of the magma system beneath Tianchi volcano, Changbaishan: phase equilibria constraints. Chin. Sci. Bull. 60, 3489–3500 (in Chinese).
Guo, W.F., Liu, J.Q., Wu, C.L., Lei, M., Qin, H.P., Wang, N., Zhang, X., Chen, H.J., Wang, Z., 2016. Petrogenesis of trachyte and the felsic magma system at Tianchi volcano: trace elements and isotopic constraints. Geol. Rev. 62, 617–630 (in Chinese).
Hartmann, J., Moosdorf, N., 2012. The new global lithological map database GLiM: a representation of rock properties at the Earth surface. Geochem. Geophys. Geosyst. 13.
Hartmann, J., Jansen, N., Durr, H.H., Kempe, S., Kohler, P., 2009. Global CO_2-consumption by chemical weathering: what is the contribution of highly active weathering regions? Glob. Planet. Chang. 69, 185–194.
Henderson, G.S., Calas, G., Stebbins, J.F., 2006. The structure of silicate glasses and melts. Elements 2, 269–273.
Hsu, C.N., Chen, J.C., Ho, K.S., 2000. Geochemistry of Cenozoic volcanic rocks from Kirin Province, Northeast China. Geochem. J. 34, 33–58.
Huang, J., Zhao, D., 2006. High-resolution mantle tomography of China and surrounding regions. J. Geophys. Res. 111.
Huang, F., Chakraborty, P., Lundstrom, C.C., Holmden, C., Glessner, J.J.G., Kieffer, S.W., Lesher, C.E., 2010. Isotope fractionation in silicate melts by thermal diffusion. Nature 464, 396–400.
Huang, K.J., Teng, F.-Z., Wei, G.J., Ma, J.L., Bao, Z.Y., 2012. Adsorption- and desorption-controlled magnesium isotope fractionation during extreme weathering of basalt in Hainan Island, China. Earth Planet. Sci. Lett. 359, 73–83.
Huang, F., Chen, L.J., Wu, Z.Q., Wang, W., 2013. First-principles calculations of equilibrium Mg isotope fractionations between garnet, clinopyroxene, orthopyroxene, and olivine: Implications for Mg isotope thermometry. Earth Planet. Sci. Lett. 367, 61–70.
Huang, J., Ke, S., Gao, Y.J., Xiao, Y.L., Li, S.G., 2015. Magnesium isotopic compositions of altered oceanic basalts and gabbros from IODP site 1256 at the East Pacific Rise. Lithos 231, 53–61.
Ibarra, D.E., Caves, J.K., Moon, S., Thomas, D.L., Hartmann, J., Chamberlain, C.P., Maher, K., 2016. Differential weathering of basaltic and granitic catchments from concentration–discharge relationships. Geochim. Cosmochim. Acta 190, 265–293.
Jiang, H.C., Ding, Z.L., 2008. A 20 Ma pollen record of East-Asian summer monsoon evolution from Guyuan, Ningxia, China. Palaeogeogr. Palaeoclimatol. Palaeoecol. 265, 30–38.
Jin, B.L., Zhang, X.Y., 1994. Researching Volcanic Geology in Changbai Mt Northeast Korea (in Chinese). Nation Education Press, Yanbian, pp. 1–223 (in Chinese).
Ke, S., Teng, F.-Z., Li, S.G., Gao, T., Liu, S.A., He, Y.S., Mo, X.X., 2016. Mg, Sr, and O isotope geochemistry of syenites from northwest Xinjiang, China: tracing carbonate recycling during Tethyan oceanic subduction. Chem. Geol. 437, 109–119.
Kent, D.V., Muttoni, G., 2013. Modulation of late cretaceous and Cenozoic climate by variable drawdown of atmospheric pCO_2 from weathering of basaltic provinces on continents drifting through the equatorial humid belt. Clim. Past 9, 525–546.
Kuritani, T., Kimura, J.I., Miyamoto, T., Wei, H.Q., Shimano, T., Maeno, F., Jin, X., Taniguchi, H., 2009. Intraplate magmatism related to deceleration of upwrelling asthenospheric mantle: implications from the Changbaishan shield basalts, northeast China. Lithos 112, 247–258.
Kuritani, T., Ohtani, E., Kimura, J.I., 2011. Intensive hydration of the mantle transition zone beneath China caused by ancient slab stagnation. Nat. Geosci. 4, 713–716.
Kurschner, W.M., Kvacek, Z., Dilcher, D.L., 2008. The impact of Miocene atmospheric carbon dioxide fluctuations on climate and the evolution of terrestrial ecosystems. Proc. Natl. Acad. Sci. 105, 449–453.
Kurtz, A.C., Derry, L.A., Chadwick, O.A., 2001. Accretion of Asian dust to Hawaiian soils: Isotopic, elemental, and mineral mass balances. Geochim. Cosmochim. Acta 65, 1971–1983.
Langmuir, C.H., Bender, J.F., Bence, A.E., Hanson, G.N., Taylor, S.R., 1977. Petrogenesis of Basalts from the Famous Area: Mid-Atlantic Ridge. Earth Planet. Sci. Lett. 36, 133–156.
Larsen, H.C., Saunders, A.D., Clift, P.D., Beget, J., Wei, W., Spezzaferri, S., 1994. Seven million years of glaciation in Greenland. Science 264, 952–955.
Li, N., Fan, Q.C., Sun, Q., Zhang, W.L., 2004. Magma evolution of Changbaishan Tianchi volcano: evidences from the main phenocrystal minerals. Acta Petrol. Sin. 20, 575–582 (in Chinese).
Li, W.Y., Teng, F.-Z., Ke, S., Rudnick, R.L., Gao, S., Wu, F.Y., Chappell, B.W., 2010. Heterogeneous magnesium isotopic composition of the upper continental crust. Geochim. Cosmochim. Acta 74, 6867–6884.
Li, C.F., Chu, Z.Y., Guo, J.H., Li, Y.L., Yang, Y.H., Li, X.H., 2015. A rapid single column separation scheme for high precision Sr–Nd–Pb isotopic analysis in geological samples using thermal ionization mass spectrometry. Anal. Methods 7, 4793–4802.
Li, G.J., Hartmann, J., Derry, L.A., West, A.J., You, C.F., Long, X., Zhan, T., Li, L., Li, G., Qiu, W., Li, T., Liu, L., Chen, Y., Ji, J., Zhao, L., Chen, J., 2016a. Temperature dependence of basalt weathering. Earth Planet. Sci. Lett. 443, 59–69.
Li, C.F., Wang, X.C., Guo, J.H., Chu, Z.Y., Feng, L.J., 2016b. Rapid separation scheme of Sr, Nd, Pb and Hf from a single rock digest using a tandem chromatography column prior to isotope ratio measurements by mass spectrometry. J. Anal. At. Spectrom. 31, 1150–1159.
Li, S.G., Yang, W., Ke, S., Meng, X.N., Tian, H.C., Xu, L.J., He, Y.S., Huang, J., Wang, X.C., Xia, Q.K., Sun, W.D., Yang, X.Y., Ren, Z.Y., Wei, H.Q., Liu, Y.S., Meng, F.C., Yan, J., 2017. Deep carbon cycles constrained by a large-scale mantle Mg isotope anomaly in eastern China. Nat. Sci. Rev. 4, 111–120.
Liu, J.Q., 1999. Volcanoes in China. Science Press, Beijing, pp. 1–219 (in Chinese).
Liu, R.X., 2000. Active Volcanoes in China (in Chinese). Seismological Press, Beijing, pp. 1–114 (in Chinese).
Liu, J.Q., Wang, S.S., 1982. Age of Changbaishan Volcano and Tianchi Lake. Chin. Sci. Bull. 1312-1315 (in Chinese).
Liu, R.X., Qiu, S.H., Cai, L.Z., Wei, H.Q., Yang, Q.F., Xian, Z.Q., Bo, G.C., Zhong, J., 1998. The date of last large eruption of Changbaishan-Tianchi volcano and its significance. Sci. China 41, 69–74 (in Chinese).
Liu, S.A., Teng, F.-Z., He, Y.S., Ke, S., Li, S.G., 2010. Investigation of magnesium isotope fractionation during granite differentiation: implication for Mg isotopic composition of the continental crust. Earth Planet. Sci. Lett. 297, 646–654.
Liu, S.A., Teng, F.-Z., Yang, W., Wu, F.Y., 2011. High-temperature inter-mineral magnesium isotope fractionation in mantle xenoliths from the North China craton. Earth Planet. Sci. Lett. 308, 131–140.
Liu, X.M., Rudnick, R.L., McDonough, W.F., Cummings, M.L., 2013. Influence of chemical weathering on the composition of the continental crust: insights from Li and Nd isotopes in bauxite profiles developed on Columbia River Basalts. Geochim. Cosmochim. Acta 115, 73–91.
Liu, X.M., Teng, F.-Z., Rudnick, R.L., McDonough, W.F., Cummings, M.L., 2014. Massive magnesium depletion and isotope fractionation in weathered basalts. Geochim. Cosmochim. Acta 135, 336–349.
Liu, J.Q., Chen, S.S., Guo, Z.F., Guo, W.F., He, H.Y., You, H.T., Kim, H.M., Sung, G.H., Kim, H., 2015. Geological background and geodynamic mechanism of Mt. Changbai volcanoes on the China–Korea border. Lithos 236-237, 46–73.
Louvat, P., Allègre, C.J., 1997. Present denudation rates at Réunion island determined by river geochemistry: basalt weathering and mass budget between chemical and mechanical erosions. Geochim. Cosmochim. Acta 61, 3645–3669.
Louvat, P., Allègre, C.J., 1998. Riverine erosion rates on Sao Miguel volcanic island, Azores archipelago. Chem. Geol. 148, 177–200.
Ma, J.L., 2011. Elemental and Isotopic Systematics During Intensive Chemical Weathering of Basalts: Variabilities and Their Mechanisms. Phd Thesis. Guangzhou Institute of Geochemistry, Chinese Academy of Sciences, Guangzhou, pp. 1–108 (in Chinese).
Ma, J.L., Wei, G.J., Xu, Y.G., Long, W.G., Sun, W.D., 2007. Mobilization and re-distribution of major and trace elements during extreme weathering of basalt in Hainan Island, South China. Geochim. Cosmochim. Acta 71, 3223–3237.
Ma, J.L., Wei, G.J., Xu, Y.G., Long, W.G., 2010. Variations of Sr–Nd–Hf isotopic systematics in basalt during intensive weathering. Chem. Geol. 269, 376–385.
Ma, H.R., Yang, Q.F., Pan, X.D., Wu, C.Z., Chen, C., 2015. Origin of early Pleistocene basaltic lavas in the Erdaobaihe river basin, Changbaishan region. Acta Petrol. Sin. 31, 3484–3494 (in Chinese).
McCulloch, M.T., Gregory, R.T., Wasserburg, G.J., Taylor, H.P., 1981. Sm-Nd, Rb-Sr, and $^{18}O/^{16}O$ isotopic systematics in an oceanic crustal section: evidence from the Samail Ophiolite. J. Geophys. Res. 86, 2721–2735.
McDonough, W.F., Sun, S.S., 1995. The Composition of the Earth. Chem. Geol. 120, 223–253.
Meng, X.Q., Liu, L.W., Wang, X.T., Balsam, W., Chen, J., Ji, J.F., 2018. Mineralogical evidence of reduced East Asian summer monsoon rainfall on the Chinese loess plateau during the early Pleistocene interglacials. Earth Planet. Sci. Lett. 486, 61–69.
Moon, S., Chamberlain, C.P., Hilley, G.E., 2014. New estimates of silicate weathering rates and their uncertainties in global rivers. Geochim. Cosmochim. Acta 134, 257–274.
Negrel, P., 2006. Water-granite interaction: clues from strontium, neodymium and rare earth elements in soil and waters. Appl. Geochem. 21, 1432–1454.
Nesbitt, H.W., Young, G.M., 1982. Early Proterozoic Climates and Plate Motions Inferred from Major Element Chemistry of Lutites. Nature 299, 715–717.
Nesbitt, H.W., Markovics, G., Price, R.C., 1980. Chemical processes affecting alkalis and alkaline earths during continental weathering. Geochim. Cosmochim. Acta 44, 1659–1666.
Opfergelt, S., Georg, R.B., Delvaux, B., Cabidoche, Y.M., Burton, K.W., Halliday, A.N., 2012. Mechanisms of magnesium isotope fractionation in volcanic soil weathering sequences, Guadeloupe. Earth Planet. Sci. Lett. 341, 176–185.
Park, S.C., Kim, T.U., Cho, I.W., Kim, S.C., Kim, I.C., 2016. Scoriae magma evolution at Paekdu volcano, Democratic People's Republic of Korea. Acta Petrol. Sin. 32, 3214–3224 (in Chinese).
Price, R.C., Gray, C.M., Wilson, R.E., Frey, F.A., Taylor, S.R., 1991. The effects of weathering on rare-earth element, Y and Ba abundances in tertiary basalts from southeastern Australia. Chem. Geol. 93, 245–265.
Ramos, F.C., Heizler, M.T., Buettner, J.E., Gill, J.B., Wei, H.Q., Dimond, C.A., Scott, S.R., 2016. U-series and $^{40}Ar/^{39}Ar$ ages of Holocene volcanic rocks at Changbaishan volcano, China. Geology 44, 511–514.
Richter, F.M., Watson, E.B., Mendybaev, R., Dauphas, N., Georg, B., Watkins, J., Valley, J., 2009. Isotopic fractionation of the major elements of molten basalt by chemical and thermal diffusion. Geochim. Cosmochim. Acta 73, 4250–4263.
Rudnick, R.L., Gao, S., 2003. Composition of the continental crust. Treatise Geochem. 3, 1–64.
Shao, F.L., Niu, Y.L., Regelous, M., Zhu, D.-C., 2015. Petrogenesis of peralkaline rhyolites in an intra-plate setting: Glass House Mountains, southeast Queensland, Australia. Lithos 216-217, 196–210.
Shen, B., Jacobsen, B., Lee, C.T.A., Yin, Q.Z., Morton, D.M., 2009. The Mg isotopic systematics of granitoids in continental arcs and implications for the role of chemical weathering in crust formation. Proc. Natl. Acad. Sci. 106, 20652–20657.
Stewart, B.W., Capo, R.C., Chadwick, O.A., 2001. Effects of rainfall on weathering rate, base cation provenance, and Sr isotope composition of Hawaiian soils. Geochim. Cosmochim. Acta 65, 1087–1099.
Su, B.X., Hu, Y., Teng, F.Z., Xiao, Y., Zhou, X.H., Sun, Y., Zhou, M.F., Chang, S.C., 2017.

Magnesium isotope constraints on subduction contribution to Mesozoic and Cenozoic East Asian continental basalts. Chem. Geol. 466, 116–122.
Sun, S.S., McDonough, W.F., 1989. Chemical and isotopic systematics of oceanic basalts: implications for mantle composition and processes. Geol. Soc. Lond., Spec. Publ. 42, 313–345.
Sun, C.Q., Wei, H.Q., Liu, Q., Pan, X.D., 2008. K-Ar dating on the trachytes composing the Tianchi composite cone in Changbaishan. Seismol. Geol. 30, 484–496 (in Chinese).
Sun, Y.B., Ma, L., Bloemendal, J., Clemens, S., Qiang, X.K., An, Z.S., 2015. Miocene climate change on the Chinese Loess Plateau: possible links to the growth of the northern Tibetan Plateau and global cooling. Geochem. Geophys. Geosyst. 16, 2097–2108.
Sun, Y., Teng, F.-Z., Ying, J.F., Su, B.X., Hu, Y., Fan, Q.C., Zhou, X.H., 2017. Magnesium isotopic evidence for ancient subducted oceanic crust in LOMU-Like potassium-rich volcanic rocks. J. Geophys. Res. 122, 7562–7572.
Sun, H., Xiao, Y., Gao, Y., Zhang, G., Casey, J.F., Shen, Y., 2018. Rapid enhancement of chemical weathering recorded by extremely light seawater lithium isotopes at the Permian–Triassic boundary. Proc. Natl. Acad. Sci. 115, 3782–3787.
Tang, Y.C., Obayashi, M., Niu, F.L., Grand, S.P., Chen, Y.J., Kawakatsu, H., Tanaka, S., Ning, J.Y., Ni, J.F., 2014. Changbaishan volcanism in northeast China linked to subduction-induced mantle upwelling. Nat. Geosci. 7, 470–475.
Teng, F.-Z., 2017. Magnesium Isotope Geochemistry. Rev. Mineral. Geochem. 82, 219–287.
Teng, F.-Z., Wadhwa, M., Helz, R.T., 2007. Investigation of magnesium isotope fractionation during basalt differentiation: implications for a chondritic composition of the terrestrial mantle. Earth Planet. Sci. Lett. 261, 84–92.
Teng, F.-Z., Li, W.Y., Ke, S., Marty, B., Dauphas, N., Huang, S.C., Wu, F.Y., Pourmand, A., 2010. Magnesium isotopic composition of the Earth and chondrites. Geochim. Cosmochim. Acta 74, 4150–4166.
Teng, F.-Z., Yang, W., Rudnick, R.L., Hu, Y., 2013. Heterogeneous magnesium isotopic composition of the lower continental crust: a xenolith perspective. Geochem. Geophys. Geosyst. 14, 3844–3856.
Teng, F.-Z., Li, W.Y., Ke, S., Yang, W., Liu, S.A., Sedaghatpour, F., Wang, S.J., Huang, K.J., Hu, Y., Ling, M.X., Xiao, Y., Liu, X.M., Li, X.W., Gu, H.O., Sio, C.K., Wallace, D.A., Su, B.X., Zhao, L., Chamberlin, J., Harrington, M., Brewer, A., 2015. Magnesium Isotopic Compositions of International Geological Reference Materials. Geostand. Geoanal. Res. 39, 329–339.
Tian, H.-C., Yang, W., Li, S.G., Ke, S., Chu, Z.Y., 2016. Origin of low δ^{26}Mg basalts with EM-I component: evidence for interaction between enriched lithosphere and carbonated asthenosphere. Geochim. Cosmochim. Acta 188, 93–105.
Wang, S.J., Teng, F.-Z., Rudnick, R.L., Li, S.G., 2015. The behavior of magnesium isotopes in low-grade metamorphosed mudrocks. Geochim. Cosmochim. Acta 165, 435–448.
Wang, X.J., Chen, L.H., Hofmann, A.W., Mao, F.G., Liu, J.Q., Zhong, Y., Xie, L.W., Yang, Y.H., 2017. Mantle transition zone-derived EM1 component beneath NE China: geochemical evidence from Cenozoic potassic basalts. Earth Planet. Sci. Lett. 465, 16–28.
Wei, H., Sparks, R.S.J., Liu, R., Fan, Q., Wang, Y., Hong, H., Zhang, H., Chen, H., Jiang, C., Dong, J., Zheng, Y., Pan, Y., 2003. Three active volcanoes in China and their hazards. J. Asian Earth Sci. 21, 515–526.
Wei, H.Q., Wang, Y., Jin, J.Y., Gao, L., Yun, S.H., Jin, B.L., 2007. Timescale and evolution of the intracontinental Tianchi volcanic shield and ignimbrite-forming eruption, Changbaishan, Northeast China. Lithos 96, 315–324.
Wilding, M.C., Benmore, C.J., Tangeman, J.A., Sampath, S., 2004. Evidence of different structures in magnesium silicate liquids: coordination changes in forsterite- to enstatite-composition glasses. Chem. Geol. 213, 281–291.
Wimpenny, J., Yin, Q.Z., Tollstrup, D., Xie, L.W., Sun, J., 2014. Using Mg isotope ratios to trace Cenozoic weathering changes: a case study from the Chinese Loess Plateau. Chem. Geol. 376, 31–43.
Xiao, Y., Teng, F.-Z., Zhang, H.F., Yang, W., 2013. Large magnesium isotope fractionation in peridotite xenoliths from eastern North China craton: product of melt-rock interaction. Geochim. Cosmochim. Acta 115, 241–261.
Xie, G.H., Wang, J.W., Basu, A.R., Tatsumoto, M., 1988. Petrochemistry and Sr, Nd, Pb isotopic geochemistry of Cenozoic volcanic rocks, Changbaishan area, northeast China. Acta Petrol. Sin. 1-13 (in Chinese).
Yang, W., Teng, F.-Z., Zhang, H.F., Li, S.G., 2012. Magnesium isotopic systematics of continental basalts from the North China craton: implications for tracing subducted carbonate in the mantle. Chem. Geol. 328, 185–194.
Yang, W., Teng, F.-Z., Li, W.Y., Liu, S.A., Ke, S., Liu, Y.S., Zhang, H.F., Gao, S., 2016. Magnesium isotopic composition of the deep continental crust. Am. Mineral. 101, 243–252.
Yang, J.H., Cawood, P.A., Du, Y.S., Condon, D.J., Yan, J.X., Liu, J.Z., Huang, Y., Yuan, D.X., 2018. Early Wuchiapingian cooling linked to Emeishan basaltic weathering? Earth Planet. Sci. Lett. 492, 102–111.
Young, E.D., Galy, A., 2004. The isotope geochemistry and cosmochemistry of magnesium. Rev. Mineral. Geochem. 55, 197–230.
Zachos, J., Pagani, M., Sloan, L., Thomas, E., Billups, K., 2001. Trends, rhythms and aberrations in global climate 65 Ma to present. Science 292, 686–693.
Zhang, C.K., Zhang, X.K., Zhao, J.R., Liu, B.F., Zhang, J.S., Yang, Z.X., Sun, G.W., 2002. Crust-mantle structure of the Changbaishan Tianchi volcanic region and its vicinity: an exploratory study and inferences. Chinese J. Geophys. 45, 862–871.
Zhang, M.L., Guo, Z.F., Liu, J.Q., Liu, G.M., Zhang, L.H., Lei, M., Zhao, W.B., Ma, L., Sepe, V., Ventura, G., 2018. The intraplate Changbaishan volcanic field (China/North Korea): a review on eruptive history, magma genesis, geodynamic significance, recent dynamics and potential hazards. Earth Sci. Rev. 187, 19–52.
Zhao, D.P., Tian, Y., Lei, J., Liu, L.C., Zheng, S.H., 2009. Seismic image and origin of the Changbai intraplate volcano in East Asia: role of big mantle wedge above the stagnant Pacific slab. Phys. Earth Planet. Inter. 173, 197–206.
Zindler, A., Hart, S., 1986. Chemical geodynamics. Annu. Rev. Earth Planet. Sci. 14, 493–571.
Zou, H.B., Reid, M.R., Liu, Y.S., Yao, Y.P., Xu, X.S., Fan, Q.C., 2003. Constraints on the origin of historic potassic basalts from northeast China by U-Th disequilibrium data. Chem. Geol. 200, 189–201.
Zou, H.B., McKeegan, K.D., Xu, X.S., Zindler, A., 2004. Fe-Al-rich tridymite–hercynite xenoliths with positive cerium anomalies: preserved lateritic paleosols and implications for Miocene climate. Chem. Geol. 207, 101–116.
Zou, H.B., Fan, Q.C., Yao, Y.P., 2008. U-Th systematics of dispersed young volcanoes in NE China: asthenosphere upwelling caused by piling up and upward thickening of stagnant Pacific slab. Chem. Geol. 255, 134–142.
Zou, H.B., Fan, Q.C., Zhang, H.F., 2010. Rapid development of the great Millennium eruption of Changbaishan (Tianchi) Volcano, China/North Korea: evidence from U-Th zircon dating. Lithos 119, 289–296.
Zou, H.B., Fan, Q.C., Zhang, H.F., Schmitt, A.K., 2014. U-series zircon age constraints on the plumbing system and magma residence times of the Changbai volcano, China/North Korea border. Lithos 200, 169–180.